# Irradiation Growth of Zirconium Alloys
# A Review

*Authors*

Ronald Adamson
Fremont, CA, USA


Malcolm Griffiths
Deep River, Ontario, Canada


Charles Patterson
Clovis, CA, USA


*Technical Editor*

Ronald Adamson
Fremont, CA, USA

**A.N.T. INTERNATIONAL®**

Ecolabelled printed matter, 4041 0799

# Disclaimer

The information presented in this report has been compiled and analysed by
Advanced Nuclear Technology International Europe AB (ANT International®) and its subcontractors.
ANT International has exercised due diligence in this work, but does not warrant the accuracy or
completeness of the information. ANT International does not assume any responsibility for any
consequences as a result of the use of the information for any party, except a warranty
for reasonable technical skill, which is limited to the amount paid for this report.

## Quality-checked and authorized by:

Mr Peter Rudling, President of ANT International

# Contents

# Summary/Perspective

Irradiation growth is a change in the dimensions of a zirconium alloy reactor component even though the applied stress is nominally zero. It is approximately a constant volume process, so if there is, for example, an increase in the length of a component, the width and/or thickness must decrease to maintain constant volume. Understanding of the detailed mechanism is still evolving; however a clear correlation of growth to microstructure evolution exists, and many empirical observations have revealed key mechanistic aspects. The inherent anisotropy of the Zr crystallographic structure plays a strong role in the mechanism, as materials with isotropic crystallographic structure (like stainless steel, copper, Inconel, etc.) do not undergo irradiation growth, unless there is an anisotropic dislocation structure. It is not to be confused with irradiation swelling, which does not conserve volume and does not occur in zirconium alloys under normal reactor operating conditions.

Irradiation growth in Zr-alloys is strongly affected by fluence, CW, texture, irradiation temperature, and material chemistry (alloying and impurity elements). Each of these factors has been reviewed in this STR. The literature review concentrates on parameters of temperature, fluence and alloying elements relevant to current commercial power reactors. However, when other data are useful, for instance very high or very low temperature, they are incorporated. And, the authors' viewpoints and analyses are sprinkled liberally throughout.

The shape of the fluence versus irradiation growth curve for a particular alloy has in general been well defined. After an initial transient that is generally small (~0.01%), the growth rate as a function of dose in recrystallized (RXA) materials is low with texture dependent strains in the long (longitudinal, axial) directions on the order of 0.05 to 0.10% for fluences up to about 1 to 2 x $10^{26}$ n.m$^{-2}$ (between 15 and 30 dpa). At some critical incubation fluence range, which is influenced by temperature and alloy composition, the growth rate increases significantly, and can even exceed the rate for cold worked material. It is in this "breakaway" growth regime where flux/fluence gradients can result in, for instance, reactor component bowing. On the other hand, growth in cold-worked stress-relieved (SRA) materials is high starting at very low fluences, with growth rates approximately the same, or even lower than, post-breakaway RXA materials. High growth rates are associated with the existence of microstructural features--- for RXA the creation of an anisotropic distribution of radiation-induced dislocation loops lying on basal planes (<c> component dislocation loops) and on prism planes (<a> component dislocation loops), and for cold-worked material the existence of <c> component dislocations in the as-fabricated state plus the radiation-induced <c> and <a> component loops. Alloy composition has a major influence on initiation of <c> component loops; in particular, niobium (Nb) containing alloys can resist formation of <c> component loops, therefore resisting high rates of breakaway growth until fluences approaching the normal lifetime of many components.

Although much is now known, to truly optimize irradiation growth behaviour additional careful single-parameter experimental studies are needed, along with enhanced mechanistic understanding, which requires increased facilities (including computer based simulations) and funding.

This report also addresses understanding of what factors control irradiation growth in Zr-alloys, based on a consideration of irradiation deformation mechanisms and application of rate-theory models. Fundamentally, it has been assumed that steady state irradiation growth is primarily dictated by diffusional mass transport, with the understanding that there may be long transients caused by the relaxation of inter-granular stresses. These stresses may arise from cold-working and high temperature heat treatments, and they can be relieved to some extent by low temperature stress-relief heat treatments. The strain arising from the relaxation of inter-granular stresses occurs by a creep mechanism involving dislocation slip in addition to mass transport (point defect diffusion) during irradiation. This creep process contributes to the mechanism of the initial "growth" transient observed. In the absence of an applied external stress, and especially for annealed materials, irradiation growth is deemed to be dependent primarily on the intrinsic diffusion of radiation-induced point defects and the density and distribution of point defect sinks in the microstructure.

The main factors controlling steady-state irradiation growth are listed below. Because Fe, which is a minor alloying element, and is also a common impurity element in Zr, is both ubiquitous and ambiguous in its effect on irradiation growth, it deserves special attention.

1. Irradiation damage (expressed as displacements per atom) is the primary driver of irradiation growth. The atomic displacement damage rate is the rate of creation of point defects and is a function of the neutron flux. To a large extent the damage rate is proportional to the fast neutron flux (often quoted as E > 0.1 MeV or E > 1 Mev). The relationship between fast neutron flux and dpa rate is nearly the same (within about 10%) for most thermalized nuclear reactors. Only in cases where the neutron spectrum differs significantly (thermal compared with fast reactors such as BOR-60 and EBR-II) does the proportionality factor change significantly.

2. The temperature dependence of irradiation growth is largely dependent on the alloy. Annealed Zr and ZrSn alloys tend to have a positive temperature dependence at temperatures below about 450 °C where dislocation network and loop recovery is not significant. The positive temperature dependence observed for the Zircaloys is largely because basal plane c-component loops and breakaway growth are more prevalent at higher temperatures. Cold-worked SRA Zr-2.5wt%Nb alloys exhibit a negative temperature dependence that may, in part, be linked with the effect of recovery of residual stresses and perhaps a change in diffusional anisotropy.

3. Alloying elements such as Nb have a profound effect on reducing irradiation growth. When Nb is in solid solution, Zr-alloys, with or without Sn present, exhibit irradiation growth that is significantly reduced compared with unalloyed or ZrSn alloys such as Zircaloy-2 and -4. When Sn is in solution in the absence of Nb (as for EXCEL and the Zircaloys) there is a propensity for high rates of accelerated growth associated with c-component loop formation. Although microstructures of ZrNb and ZrSn alloys can often be very different, it appears that Nb may be effective in modifying the point defect properties. Rate theory modelling, where microstructure is factored in to the response of the material, shows that cascade efficiency factors of 1% and 3% give the best fits to the observations for ZrNb and ZrSn alloys respectively. This implies that point defect recombination is more effective for the ZrNb case. Recent experimental data for materials with controlled microstructures show that ZrNb alloys containing Nb in solid solution exhibit significantly lower irradiation growth compared to ZrSn alloys without Nb in solid solution.

4. Minor constituents (Fe and H in particular) can have a profound effect on the irradiation growth. Although the effect of H pick-up on the dimensional stability of reactor components is confounded by the volume swelling caused by the hydrogen, the recent results on irradiation growth show unequivocally that there is a synergistic effect of H in enhancing irradiation growth. It was demonstrated that increasing the Fe content has a significant effect in reducing irradiation growth. The reduction in irradiation growth with increased Fe content is largely an empirical result and the mechanism by which Fe reduces growth is not immediately apparent. Characterisation of c-component loop densities in the samples studied indicates that the effect of Fe may be to suppress, or limit, c-component loop growth. Other minor constituents and impurities appear to play a more significant role in promoting c-component loop formation so Fe is likely to be acting in a way that is different from other interstitially diffusing elements. There is some evidence to suggest that c-component loops are more stable in Zr containing certain impurities (C and O for example). There is circumstantial evidence of an association with Cr because of the increased c-component loop densities in the same volume as higher dispersed Cr concentrations after irradiation. Cr is a slower interstitial diffuser compared with Fe and is thus not as readily dispersed throughout the material. Cr is thus more likely to remain in the vicinity of source precipitates at relatively high concentrations compared with Fe.

5. Microstructure ultimately plays a large role in dictating the magnitude and anisotropy of irradiation growth in Zr-alloys.

   For a given alloy composition and operating conditions, irradiation growth is strongly dependent on:

   (i) as-fabricated dislocation density and structure (degree of cold-working, a- and c-dislocation densities);

   (ii) grain size and aspect ratio;

   (iii) irradiation-induced dislocation structure (a-type and c-component loops).

Because irradiation growth is largely dependent on mass transport there has to be a balanced flow of vacancy and interstitial point defects to sinks with differing orientations. One cannot simply then consider the effect of one microstructural variable in isolation. The interplay between microstructure variables has to be studied using rate-theory formulations. Such formulations provide support for empirical relationships established through experiment and also provide some insight into the main factors affecting irradiation growth.

6. Fe is a highly mobile interstitial diffuser in Zr. Because Fe is readily dispersed during low temperature irradiation (<450 °C) it could potentially play a role in irradiation growth by interacting with either interstitial or vacancy point defects. It is conceivable that the Fe could suppress c-component loop evolution by segregating close to the dislocation core of vacancy c-component loops and inhibiting further diffusion of vacancies to these sinks. Further controlled irradiations with Zr as well as ZrSn and ZrNb alloys would help to resolve this issue

Irradiation growth is just one of the components of deformation that must be considered in the design of fuel rods and zirconium-alloy structural components. Others include creep and hydride-induced volume change. Growth is incorporated into engineering analyses by means of empirical models that reflect the in-reactor behaviour of similar materials and components. Growth has the greatest effect on the design and performance of components that are exposed to large displacements per atom (neutron fluence) and that are constrained with respect to growth; i.e., little or no space for expansion without restraint or external forces. Examples of constrained structure include guide tubes in PWR and VVER fuel assemblies, BWR fuel channels and pressure tubes in CANDU reactors. Operational issues have arisen because of irradiation and other sources of growth in all of these structures. Irradiation growth is addressed by allowing sufficient clearance to allow unimpeded dimensional changes where possible and by adopting materials that exhibit low-growth behaviour; e.g., materials and processing methods that improve creep resistance, exhibit low rates of corrosion and hydrogen pickup and low rates of irradiation growth.

While the fundamental understandings noted previously have contributed to the development of materials and their methods of fabrication, models based on first principles tend not to be used in engineering applications. Instead, design and licensing analyses typically utilize empirical correlations that are based on observations of the effects of irradiation on a material and, frequently, on specific components in the relevant operating environments. That is, separate correlations are commonly developed for each material type and heat treatment based on the observed, in-reactor behaviour of components or samples representative of fuel cladding, guide tubes, spacer/grid strip or sheet. One of the motivations for the use of models that are empirically based or that are phenomenological but based on a large number of in-reactor measurements is the need to identify the uncertainty in model predictions relative to safety limits; i.e., prediction uncertainties are more readily accepted in the design and licensing arenas when a model is based directly on the a large number of observations of the effects of in-reactor operation rather than on a set of postulates and a limited amount of experimental data. Mechanistic models can be used to assist with alloy development and material design when developing new improved components for future reactor core applications.

# 1 Introduction – Ron Adamson

## 1.1 General Dimensional Stability

Unique aspects of material behaviour in a nuclear power plant include the component's dimensional stability. In fast breeder reactors the Fe and Ni-based alloys creep and swell, that is, they change dimensions in response to a stress and change their volume in response to radiation damage. In water reactors, zirconium alloy structural components creep, do not swell, but do change their dimensions through the approximately constant volume process called irradiation growth. **Radiation effects are not unexpected since during the lifetime of a** typical fuel assembly **component every atom is displaced from its normal lattice position** at least 20 times. With very few exceptions, the mechanical and physical properties needed for reliable fuel assembly performance are affected by irradiation.

Practical effects of dimensional instabilities are well known and it is a rare technical conference in the reactor performance field that does not include discussions on the topic. In addition to lengthening due to irradiation growth, many components are subjected to creep stresses. Because of the difference in pressure inside and outside the fuel rod, cladding creeps down on the fuel early in life, and then creeps out again later in life as the fuel begins to swell. A major issue is to have creep strength sufficient to resist outward movement of the cladding if fission gas pressure becomes high at high burnups. PWR guide tubes can creep downward or laterally due to forces imposed by fuel assembly hold down forces or cross flow hydraulic forces – both leading to assembly bow which can interfere with smooth control rod motion. BWR channels can creep out or budge in response to differential water pressures across the channel wall, again leading toward control blade interference. Fuel rods, water rods or boxes, guide tubes, and tie rods all can lengthen due to irradiation growth, possibly leading to bowing problems. (For calibration, a recrystallised (RX or RXA) Zircaloy water rod or guide tube could lengthen due to irradiation growth more than 2 cm. during service; a cold worked/stress relieved (SRA) component could lengthen more than 6 cm.) Even RX spacer/grids could widen enough due to irradiation growth (if texture or heat treatment was not optimized) to cause interference with the channel.

In addition, corrosion leading to hydrogen absorption in Zircaloy can contribute to component dimensional instability due, at least in part, to the fact that the volume of zirconium hydride is about 16% larger than zirconium.

The above discussion leads to the concept that understanding the empirical details and mechanisms of dimensional instability in the aggressive environment of the nuclear core is important for very practical reasons. Reliability of materials and structure performance can depend on such understanding.

The sources of dimensional changes of reactor components (in addition to changes caused by mechanical loading, which is almost always in the elastic range, and conventional thermal expansion and contraction) are: irradiation growth, irradiation creep, thermal creep, stress relaxation (which is a combination of thermal and irradiation creep), and hydrogen and hydride formation.

Irradiation effects are primarily related to the flow of irradiation-produced defects to sinks such as grain boundaries, deformation-produced dislocations, irradiation-produced dislocation loops, and alloying and impurity element complexes. In zirconium alloys, crystallographic and diffusional anisotropy are key elements in producing dimensional changes.

In the past, hydrogen effects have been considered to be additive to and independent of irradiation; however, recent data have brought this assumption into question. It is certain that corrosion-produced hydrogen does cause significant dimensional changes simply due to the 16-17% difference in density between zirconium hydride and zirconium. A length change of on the order of 0.25% can be induced by 1000 ppm hydrogen in an unirradiated material. Recent experiments indicate that the presence of hydrogen and/or hydrides does contribute to the mechanisms of irradiation growth but probably not creep.

Fuel rod diametral changes are dominated by stress dependent creep processes, as irradiation growth in the hoop direction is very small.

Fuel rod length changes are caused by several phenomena:

– Stress free axial elongation due to irradiation growth.

– Anisotropic creep (before pellet/cladding contact) due to external reactor system pressure. Because of the tubing texture, axial elongation results from creep down of the cladding diameter; however for heavily cold worked material, it has been reported that some shrinkage may occur. In a non-textured material such as stainless steel, creep down of the cladding would only result in an increase in cladding thickness, with no change in length.

– Creep due to pellet-cladding mechanical interaction (PCMI) that results from differences in the thermal strains between fuel pellets and cladding, pellet swelling and cladding creep (closure of the pellet-cladding gap) and that increases with the intensity of contact. PCMI begins early in life due to pellet cracking and relocation in the radial direction, is moderated by the effects of pellet densification and then increases after hard contact between the cladding and fuel. This occurs in mid-life of typical LWR fuel, depending on the cladding creep properties and the dimensional stability of the fuel, and early in life for PHWR (CANDU) fuel.

– Hydriding of the cladding due to corrosion.

Bow of a component such as a BWR channel or PWR control rod assembly can occur if one side of the component changes length more than the other side. Such differential length changes occur due to differential stress and creep, to relaxation of differential residual stresses, or to differential irradiation growth due to differences in flux-induced fluence, texture, material cold work, and hydrogen content.

Irradiation growth occurs simultaneously with irradiation creep if there is an applied stress. The two processes are generally assumed to be independent and additive, even though they compete for the same irradiation-produced defects mechanistically. When assessing dimensional changes of any component, all sources of change must be taken into account. This is especially true for fuel rods, which will invariably have length-change components due to irradiation growth and anisotropic creep in addition to pellet-imposed stresses at higher burnups.

Irradiation creep was covered earlier by [Adamson et al., 2009].

This STR addresses all data deemed relevant to understanding irradiation growth, broad review and new aspects of growth mechanisms, and a summary of practical effects of growth on component performance.

# 1.2 Components

In-reactor dimensional stability (or in-stability!) affects the dimensions of all Zirconium-alloy components during exposure in the core of reactors. Important components and their environmental conditions include:

• The pressure tubes (PTs) of CANDU and RBMK reactors that contain the fuel assemblies (FAs). CANDU pressure tubes have a particular (tangential) basal texture and microstructure governed by ß-quenching, extrusion, and drawing. They operate at temperatures between 250 °C-310 °C under a fast flux of 0.5-3.5 x $10^{13}$ n/cm².s (>1MeV) and are stressed by the coolant pressure on the inside to a hoop stress of about 100 MPa. Target design life is 30 years at 80% capacity. For RBMK pressure tubes, the design lifetime is considerably shorter, on the order of 20 years. PT material is Zr2.5Nb and the length is about 6m

- The thin wall fuel rod (FR) claddings of PWR/VVERs and BWRs have a radial texture governed mostly by the last rocking steps, and a medium GS (grain size) affected by intermediate annealing and cold deformation. Fuel rods are stressed by the coolant overpressure at the beginning of irradiation (compressive hoop stress of 40-80 MPa) and eventually by fuel swelling at the end of life (tensile hoop stress up to >50 MPa in SR PWR fuel rods and up to >100 MPa in Recrystallised (RXA) BWR fuel rods) and are exposed to a fast neutron flux of 0.2-2x10$^{14}$ n/cm².s. The fuel cladding can in addition, in case of fast power ramps, experience as a consequence of Pellet Cladding Interaction (PCI) rather high tensile stresses (>500 MPa) that relax quickly by in-reactor creep. The cladding outer-surface temperature is in case of BWR claddings about 290 °C and is significantly higher in case of PWR claddings, 320-360 °C. Maximum exposure times are up to 10 years for BWR fuel and up to 6 years for PWR fuel.

  FR material for BWRs is RXA Zircaloy-2 and for PWRs is SRA Zircaloy-4 or various ZrNb alloys. FR length is about 4 meters.

  For CANDUs the thin walled FR cladding tubes are Zircaloy-4 and are 0.5 m long. The required lifetime is short, about 400 days.

- The guide tubes (GT) of PWR/ VVER fuel assemblies (FAs) with a similar texture as the fuel rods provide, together with the spacers, the major structural support. However, large friction forces between the grid and fuel rods may provide some additional structural support from the fuel rods. The GT also provide the path for moving control rod cluster. The GTs are loaded axially by the hold down spring force, the hydraulic forces, the differential expansion of fuel rods and GTs and by bow forces from cross flow and neighbouring FAs. The actual forces depend on the frictional connection via the spacers between GTs and FRs and may be between several 10 MPa compressive up to several 10 MPa tensile. In addition, the GT growing oxide layer may create axial tensile stresses up to about 10 MPa. Traditionally, the GT material has been the same as for FRs, but material and heat treatment is currently being optimized for growth and creep properties.

- The water rods and capture rods for BWRs are generally the same material as the FRs, and for some designs are load bearing.

- The square BWR flow channel is the main structural component of a BWR fuel assembly bundle, providing adequate stiffness. It is the main load bearing structure during seismic events and accident conditions. It also provides a cruciform path for control blade manoeuvring. They are stressed by the difference between the coolant pressure and the pressure in the outer bypass region, which increases with increasing height. They are made from strips, with the typical strip texture. Maximum stress arises at the corner (several 10 MPa tangential stress). In-reactor creep at this position results in bulging. Channels are slightly longer than the fuel rods and the materials are Zircaloy-4, Zircaloy-2 and ZrNb alloys aimed at minimizing irradiation growth. Channel lifetimes are limited by distortion (bowing, bulging, length change) that causes interference with control blade movement or decreases in thermal margins. For normal operation, lifetime can be at least as long as for FRs.

This STR aimed specifically at irradiation growth, will primarily address conditions of direct interest to LWRs and CANDUs, unless the information has mechanistic implications. Specific issues mentioned above will be addressed separately below.

More details of component characteristics are found in many ZIRAT reports, and some are summarized in [Cox et al., 2006]

## 1.3 Basics of irradiation growth

Irradiation growth is a change in the dimensions of a zirconium alloy reactor component even though the applied stress is nominally zero. It is approximately a constant volume process, so if there is, for example, an increase in the length of a component, the width and/or thickness must decrease to maintain constant volume. Understanding of the detailed mechanism is still evolving, see Section 3; however a clear correlation of growth to microstructure evolution exists, and many empirical

observations have revealed key mechanistic aspects. The inherent anisotropy of the Zr crystallographic structure plays a strong role in the mechanism, as materials with isotropic crystallographic structure (like stainless steel, copper, Inconel, etc.) do not undergo irradiation growth. It is not to be confused with irradiation swelling, which does not conserve volume and does not occur in zirconium alloys under normal reactor operating conditions.

Irradiation growth is strongly affected by fluence, cold work, texture, irradiation temperature, and material chemistry (alloying and impurity elements), as will be described in more detail in later Sections. Figure 1-1 gives schematic growth curves illustrating several points. Note that L-textured material (blue) grows, while T-textured material (red) shrinks; when taken with the third direction (N) in a component, this behaviour results in approximately constant volume. The long direction (L) of a component is the most important; for instance the length of a fuel rod, channel box or guide tube. Note that cold worked (CW) material grows at a high and almost linear rate, while recrystallised (RXA) material grows in a 3-stage process, with the final high rate being called "breakaway" growth. The various stages can be directly related to the irradiation-produced microstructure, described, example in [section 1.2, Adamson, 2000], [Rudling et al., 2007] and Sections 2 and 3 of this report. For RXA Zircaloy and most alloys, at low fluences where only <a> component loops exist, growth is small (~0.1%) and saturates with increasing fluence. When <c> component loops begin to appear (at various fluences depending on alloy) the growth rate increases. For L-texture RXA Zircaloy material, growth can reach 0.5% at 15 x $10^{25}$ n/m² (23 dpa; 75 GWd/Mt burnup). In initially cold worked (CW) or cold worked
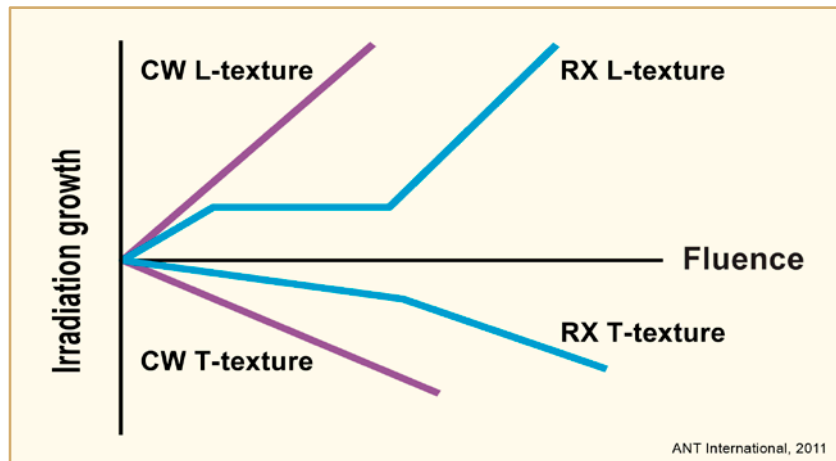


Figure 1-1:    Schematic curves for irradiation growth as a function of fluence for recrystallised (RXA) and cold worked (CW) zirconium alloys having textures characterized as L (f ≈ 0.1) and T (f ≈ 0.4) and an irradiation temperature near 300°C (573K).

stress relieved material (SRA), <c> component dislocations occur as part of the deformation-induced structure and more are formed during irradiation [Holt et al., 1996] and Section 3 of this report. The growth rate is nearly linear with fluence and the magnitude is almost linear with the amount of initial cold work. In heavily-worked material (typically 70 – 80% in a fuel rod) a growth of 0.5% can be reached by 12 dpa or about 7 x $10^{25}$ n/m². An overview of factors affecting growth is given by [Fidleris et al., 1987].

A key assumption is that irradiation growth has a linear dependence on fast flux [Holt, 2008] and section 3 of this report. Therefore growth can be plotted against fast fluence (flux x time), as is commonly done, without regard for the value of flux.

The key practical, empirical mechanistic feature of irradiation growth is the presence of <c> component dislocations (either as irradiation-produced loops or deformation-induced networks). Without them "breakaway" or accelerated growth does not occur. This is illustrated in Figure 1-2 for CW or RX Zircaloy irradiated at low (80°C (353K)) or intermediate (553K (280°C)) temperature, [Rogerson, 1988a]. For all four conditions (A, B, C, D) a high density of <a> loops forms early in life

and saturates at about $20 \times 10^{24}$ n/m². The loops at 553K (280°C) are larger than at 353K (80°C), which may account for the difference in growth magnitudes for conditions C(red) and D(green), but the effect is minor. For condition D (353K) to high fluence or condition C (553K) to less than $<40 \times 10^{24}$ n/m² there are no <c> component dislocations observed in the microstructure and growth is low.
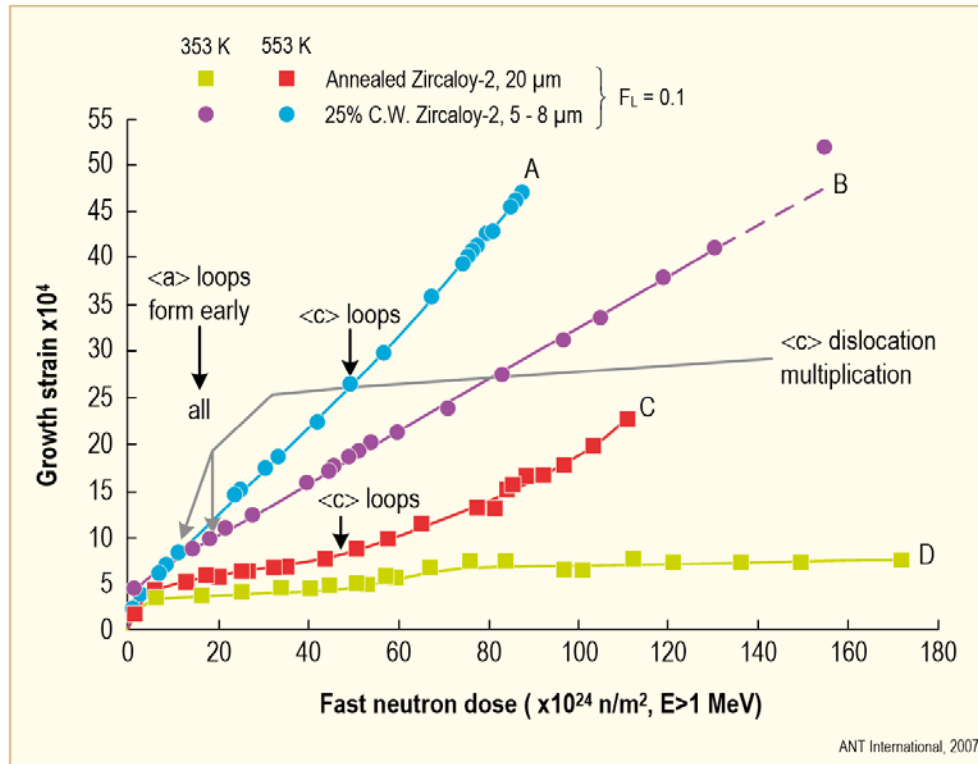


Figure 1-2:    Irradiation growth in annealed and 25% cold-worked Zircaloy-2 at 353 and 553 K [Rogerson, 1988a]. (100 = ` 17 dpa)

In condition C (553K (280°C)), <c> loops begin forming at about $40 \times 10^{24}$ n/m², at which point the growth of conditions C and D become different. No <c> loops are observed in condition D (353K (80°C)) out to high fluence [Griffiths et al., 1996].

For conditions A(blue) (553K (280°C)) and B(purple) (353K (80°C)), networks containing <c> component dislocations induced by cold work exist before irradiation, and the <c> components multiply during irradiation (by a process of helical climb with loops spreading out on the basal plane [Holt et al., 1996]. In addition, condition A (at 553K) is expected to form irradiation-induced <c> loops [Griffiths et al., 1996].

Mechanisms of growth are addressed in detail in Section 3 of this report.

An experimental measurement of increase in <c>component density as a function of fluence is shown in Figure 1-3, and the saturation of <a> loop density with fluence is shown in the upper two curves (Figure 1-4). The measurement of <c> loop density can also be done by transmission electron microscopy (TEM); however the measurement technique has many difficulties induced by the large size of the loops relative to the thickness of the TEM foil and the problems of firmly identifying loops. Figure 1-5 gives a estimate of loop density measured all by the same technique, [Mahmood et al., 2000]. Recently, [Yagnik et al., 2016] have measured, by TEM, <c> loop density out to high fluence and correlated it with growth for a number of different alloys, see sections 2 and 3 of this report.

It can be concluded that high growth rates can be correlated to the existence of <c> component dislocation loops and defects.

# 2    Data – Ron Adamson

## 2.1    Zircaloys

The shape of the general growth curves for Zircaloys is indicated in Figure 2-1 and, with more complete data, in Figure 2-2.



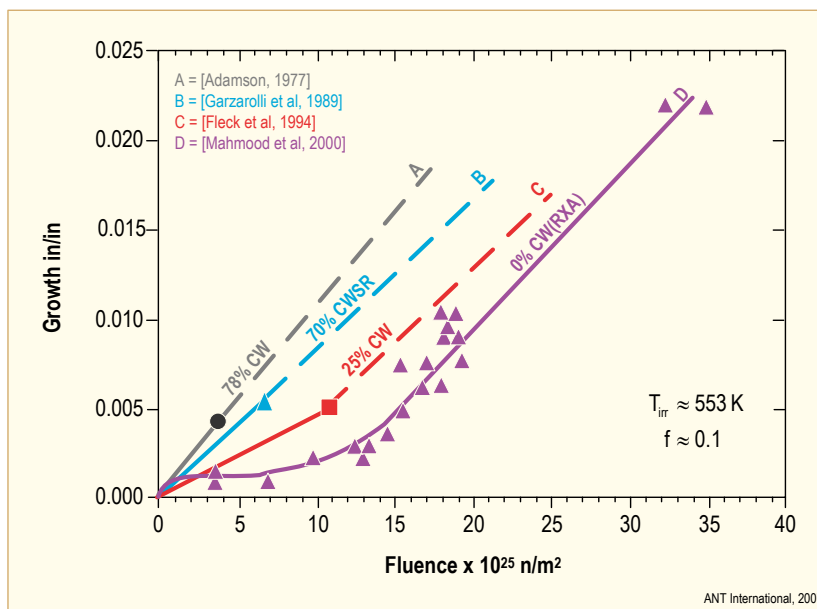Figure 2-1:    Irradiation growth in Zircaloy. Ref. A = [Adamson, 1977], Ref. B = [Garzarolli et al., 1989], Ref. C = [Fleck et al., 1994], Ref. D = [Mahmood et al., 2000]. (20 ≈31 dpa)
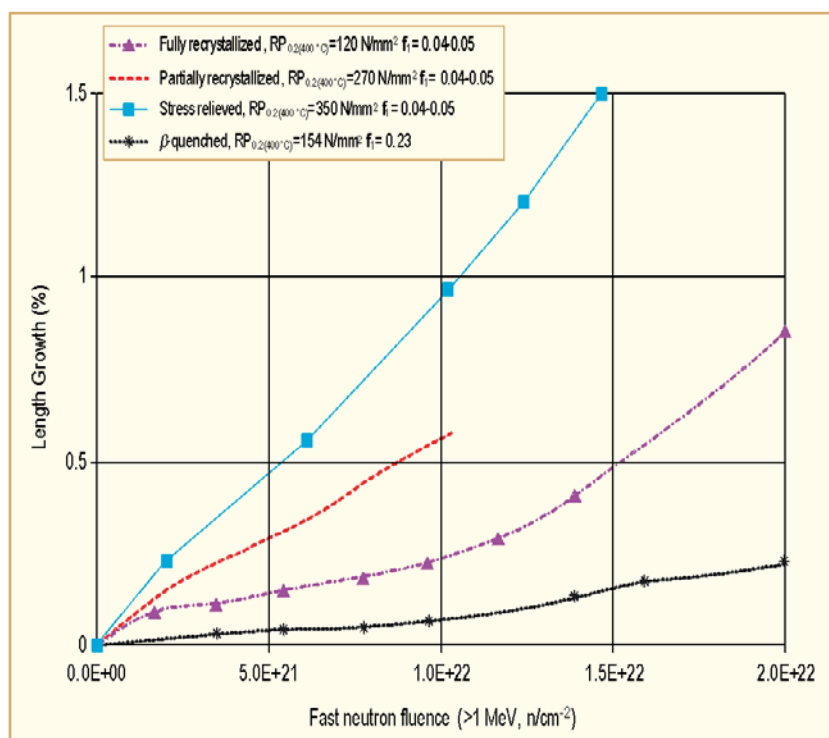


Figure 2-2:    Irradiation growth of Zircaloy at 300 °C measured on samples with different yield strength (CW, recrystallisation) and different textures ($f_1$). Data from [Garzarolli et al., 1989 and 1996]. (1.E+22 = 15 dpa)

The figures outline irradiation growth behaviour as a function of fluence for the axial direction of a typical Zircaloy fuel rod. It is noted that the growth curve is strongly affected by the presence of cold work (CW), which is defined as the percentage of cold work (deformation) after the last recrystallisation anneal of the component. For BWR fuel rods this is nominally zero, for Zircaloy-4 PWR rods it is in the range 60-80%, followed by a stress relief anneal (SRA). The primary effect of cold work considered here is to create dislocations, whose density for recrystallised (soft) material is low ($10^{11}$ per $m^2$) and for cold worked (hard) materials is high ($10^{16}$ per $m^2$). Stress relief anneal (SRA) has only a small effect on the dislocation density, while a recrystallisation anneal (RXA) reduces the density to the nominal $10^{11}$ per $m^2$ value. For an introduction to dislocations see chapter 2 in [Adamson et al., 2009]. It is seen in Figure 2-1 and Figure 2-2 and that cold work increases the growth magnitude at all fluences, but at high fluences the growth rates of SRA and RXA materials are similar. Newer data at even higher dpa show that the growth rate of RXA material may continue to increase with dpa (See section 2.3). For a 4 meter-long rod at a burnup of 50 GWd/MT (equivalent to about $10x10^{25}$ n/$m^2$(E>1 MeV)) the length change due to stress free irradiation growth would be about 0.5 cm for RX material and 3.5 cm for 70% CWSR material. At 70 GWd/MT the values are about 1.6 cm for RX and 4.7 cm for 70% CWSR. [Adamson, 1977] determined that growth is roughly proportional to the amount of cold work, and [Holt, 1979], determined that it is slightly less than linear with dislocation density, as detailed in section 2.3.

As discussed earlier, the shape of the curve is also affected by cold work and fluence. For recrystallised 0% CW material the growth magnitude appears to saturate at about 0.1% at low fluence, however, above about 25 GWd/MT burnup the growth rate increases. This "breakaway" leads to a high and increasing rate to fluences and burnups well beyond that contemplated for fuel rods. However, the growth data points at 33 x $10^{25}$ n/$m^2$ (~160 GWd/MT, 51 dpa), Figure 2-1 were obtained from actual Zircaloy structural components, so they are not beyond the realm of possibility [Mahmood et al., 2000]. At that high fluence the increase in length of a 4 meter-long RXA component could be 9 cm (3.5 inch)!

For cold worked material the growth rate is high even at the beginning of irradiation. At low fluence there may be transient lower growth rate, but within the first cycle of operation the rate reaches a value much higher than for RXA material. The rate is related to the amount of cold work and appears not to be quite linear with fluence [Holt et al., 1996], but rather to increase at higher fluences, at least for cold work amounts on the order of 25%. It is certain that at high fluences the growth rates of all Zircaloys (RXA and CW or CWSR) are high, see section 2.3.

## 2.1.1    Zircaloy-2

Four (*) Zircaloy-2 data sets useful in the analysis are given in Table 2-1. [Rogerson, 1988b], GNF and Yagnik (A30) have very low hydrogen. Mahmood specimens nominally contain 85 ppm H; however, this value is at the end of a very long irradiation, and the H concentration in the 15-25 dpa period is likely to be much lower.

Table 2-1:        Irradiation growth experiment and data.

| Reference | Material, (Sn, w/o) | Reactor | Temp, °C | Grain size, microns | Texture (fL) | H | Environment |
|---|---|---|---|---|---|---|---|
| [Garzarolli et al., 1989] | Zirc-4, (1.5) | PWR | 300 | 3-7 | 0.045 | ? | Water |
| * [Rogerson, 1988b] | Zirc-2, (1.5) | DIDO | 280 | 20 | 0.1 | 10 | Inert gas |
| *[Mahmood et al., 2000] | Zirc-2, (1.5) | PWR | 290 | 15 | 0.06 | 50-85 | Water |
| [Morize et al., 1987] | Zirc-4 (1.5) | PWR | 315 | ? | 0.19 | <50 | NaK |
| [Bossis et al., 2009] | Zirc-4 (1.3-1.5) | PWR | 315 | ? | 0.065 | <1600 | Water |
| *GNF [Kobylyansky et al., 2010] | Zirc-2, (1.3) | Fast (BOR60) | 320 | 6 | 0.09 | <50 | Na |
| *A30 [Yagnik et al., 2016] | Zirc-2 (1.3) | Fast (BOR60) | 320 | 6 | 0.1 | <50 | Na |

Since irradiation growth is caused by displaced atoms during irradiation, and since the neutron energy spectra for different reactor types is different, it is most useful to provide displace per atom (dpa) as the measure of irradiation damage rather than the conventional (n/cm², E>1 MeV), as detailed in Section 1.4. Data where this has been done are given in Table 2-2. It must be noted that for a BWR, the neutron energy spectrum is a function of the void fraction. In the case given here a mid-void (about 40%) is used.

Table 2-2:    Conversions (used by the authors) of fast fluence in various reactor types to displacements per atom (dpa). All used 40 eV as the threshold displacement energy except *Fidleris et al, who used 25 eV. Note that applying a factor of 40/25 to the Fidleris data brings it close to the other data.

| | Fluence, n/cm$^2$x10$^{20}$, E>1MeV per 1 dpa | | | | | | | | |
|---|---|---|---|---|---|---|---|---|---|
| | PWR | BWR (mid-void) | ATR | CANDU (PT) | DIDO | BOR60 | SILOE | PHENIX | EBR |
| [Gilbon & Simonot, 1994] | 7 | | | | | | 7 | 2 | |
| [Griffiths & Douglas, 2009] | 6.5 | 6.1 | 6.7 | 5.8 | | 5 | | | |
| *[Fidleris et al., 1987] | | 4.5 | 4.4 | | | | | | 2.7 |
| [Chapman et al., 1984] | | | | | 6.5 | | | | |
| [Kobylyansky et al., 2010] | | | | | | 4.8 | | | |
| [Shishov et al., 2005] | 6.0 | | | | | | | | |
| Walters et al.,2016 (this STR) | 6.5 | 6.2 | 7.0 | 5.8 | 5.9 | 4.9 | - | - | 3.2 |
| Yagnik et al., 2016 (A30) | | | | | | 5.0 | | | |
| | | | | | | | © ANT International, 2017 | | |

Figure 2-3 and Figure 2-4 give growth data versus dpa calculated from reported fluence and reactor type for the four data sets. Note that for this early data, had the Rogerson data been extrapolated to higher fluences (doses), the prediction would have been significantly low.
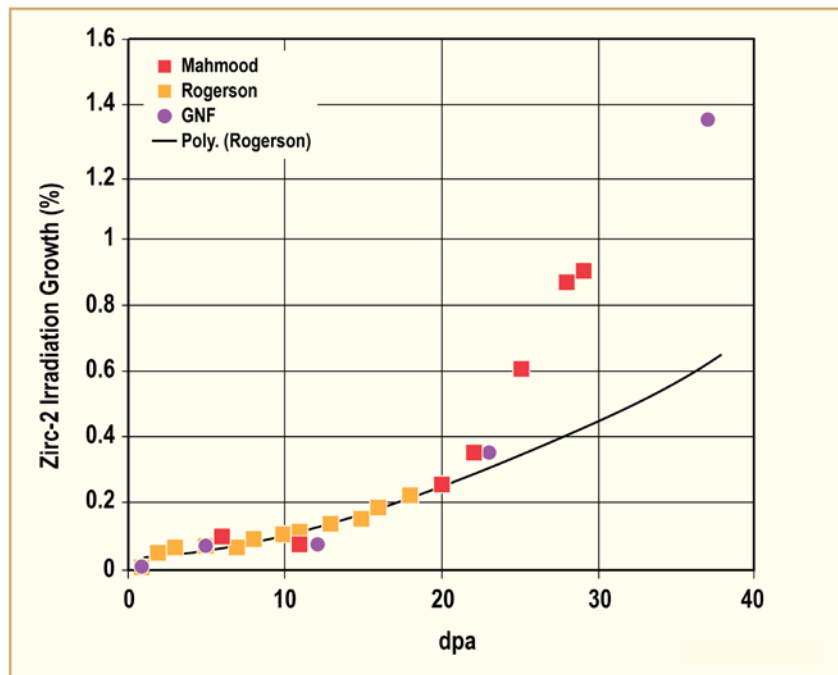


Figure 2-3:    Irradiation growth of Zircaloy-2 from experiments listed in Table 2-1.
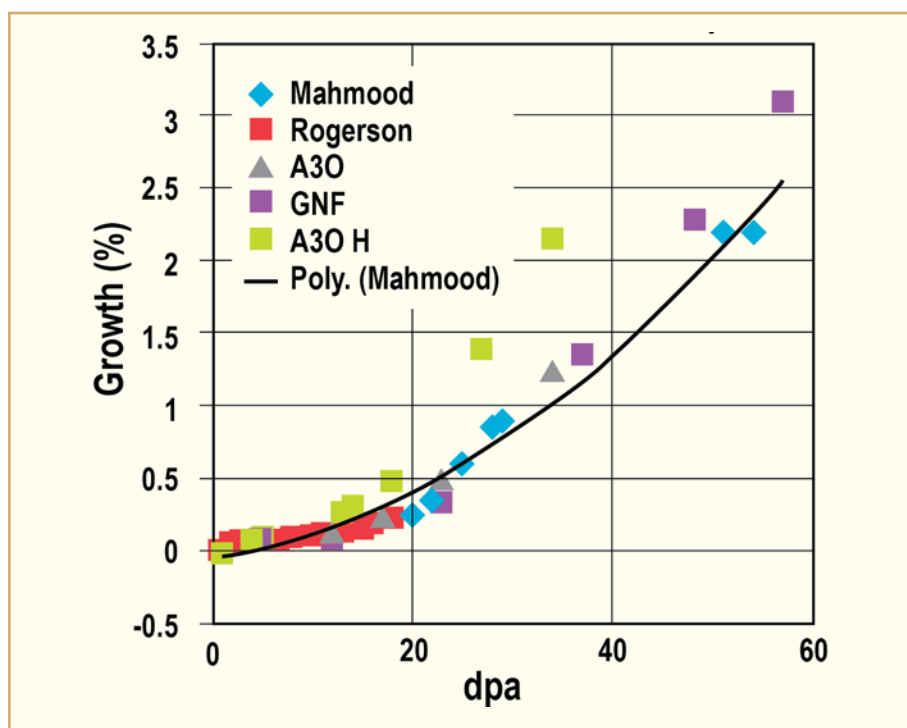
Figure 2-4:    Irradiation growth of Zircaloy-2 from experiments listed in Table 2-2.Specimen A30H has high hydrogen, see Section 2.7

Figure 2-4indicates that growth is reasonably well described for fluence (damage dose) covering the range of reactor operation interest. The obvious outlier is A30H which was pre-hydrided before irradiation, Section 2.7.

Comparison of irradiation growth data are convoluted by factors of texture, irradiation temperature, measurement technique, test environment, fluence and dpa calculation, material composition: data scatter is to be expected. Error bars are not often seen on data plots.

The texture normalization factor, (1-3f), is a rough guide to texture effects but cannot be counted on to give precise results. This factor represents the expected growth when there is a net flux of vacancies to basal planes and a net flux of interstitials to prism planes of the hcp crystal structure (see Section 3).

## 2.1.2      Zircaloy-4

Until recently, SRA Zircaloy-4 has been used for PWR cladding; however at high burnups, corrosion and hydrogen takeup is high. (CANDU reactors, with relatively low burn at discharge, continue to use Zircaloy-4 cladding) Since there is a trend to switch, at least in the short term, from Zircaloy-2 to Zircaloy-4 for BWR channel material, and since there is some early commercial data indicating high fluence gradient bow for Zircaloy-4 channels, some data is given here. In general, it is expected that growth of Zircaloy-2 and Zircaloy-4 should be similar.

Early data for low fluence, pre-breakaway growth of Zircaloy-4 is shown in Figure 2-5[Adamson, 1977]. Texture and temperature effects are evident, and the growth is low.
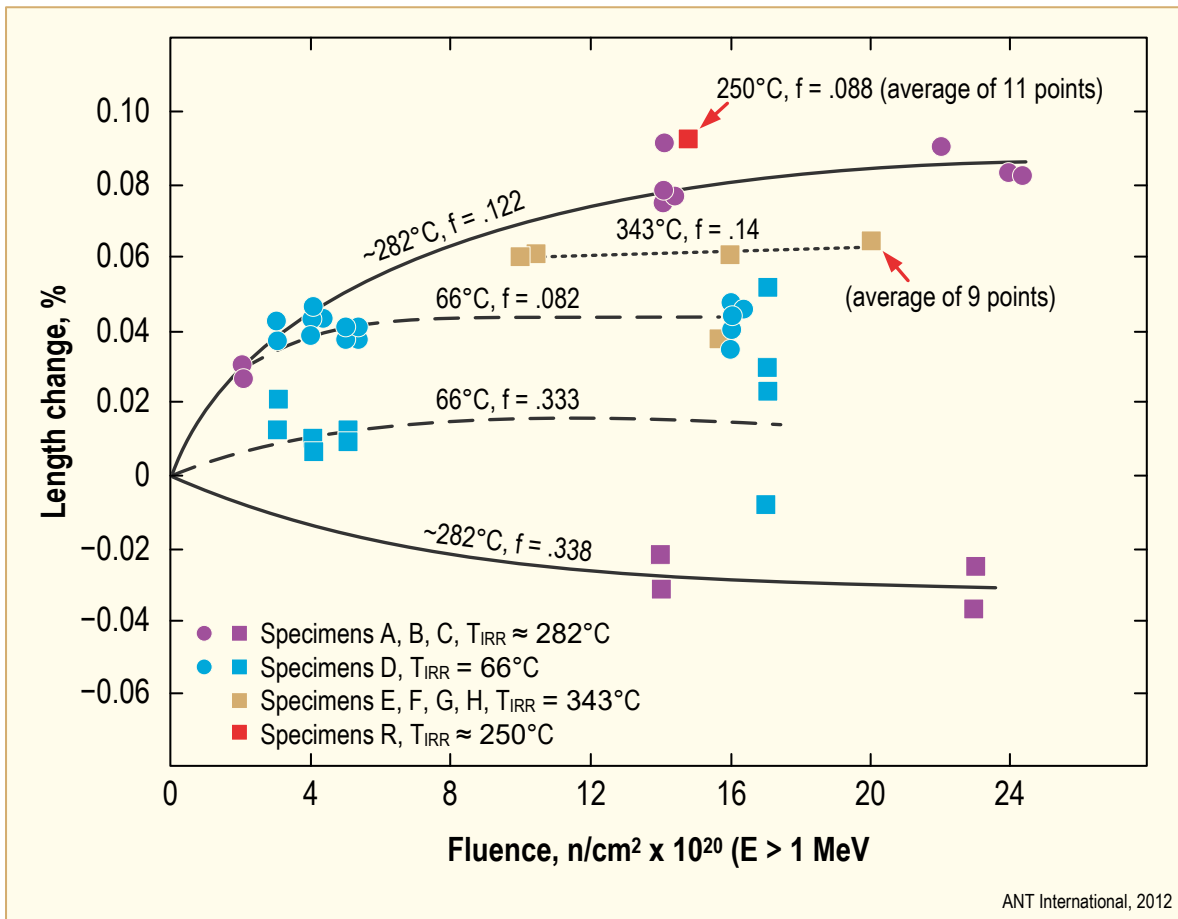
Figure 2-5:     Growth of Zircaloy-4 as functions of fluence, texture and irradiation temperature [Adamson, 1977]. (20 = 3 dpa)

In the case of BWR channels (not considered here, but in detail in ZIRAT16/IZNA11 STR [Garzarolli et al., 2011]) length change is due primarily to irradiation growth and hydride-induced volume increase; measurements cannot separate the two. Subtracting the hydride volume component using the Westinghouse or Siemens curves [King et al., 2002; Seibold et al., 2000] is appropriate, but not exact, see Section 2.7.

At low fluences (<5x10²¹ n/cm², E>1 MeV or about 9 dpa) Zircaloy-2 and -4 (as well as most other alloys) have about the same growth (.05-.10%) and a low or zero growth rate.

From Table 2-1, a comparison can be made between the two Zircaloys using older data. Data are plotted in Figure 2-6. Both [Mahmood et al., 2000] and [Garzarolli et al., 1989] data were obtained in PWRs in water near 295°C; hydrogen is not known for the Garzarolli data. It is seen that the growth curves are very similar.

# 3 Mechanisms and modelling – Malcolm Griffiths

Zirconium alloys are somewhat unique among the engineering alloys used in nuclear reactor cores in that they exhibit anisotropic dimensional changes in the absence of stress in a radiation environment. This phenomenon is known as irradiation growth. The degree to which a given structural component, with a particular microstructure, exhibits irradiation growth depends on the temperature and the atomic displacement damage rate. Irradiation growth is distinct from irradiation swelling (exhibited by steels and other structural materials) in that the volume of the material remains constant but the dimensions change at a rate proportional to the neutron flux. The anisotropy of the deformation is a function of the microstructure: crystallographic texture, grain size/shape and dislocation structure, as described in section 2. This section addresses the mechanisms of irradiation growth and provides the basis for understanding how a component made from a zirconium alloy behaves during operation in a nuclear reactor core.

## 3.1 Review of relevant data that provides insight and support for mechanistic models

### 3.1.1 Power reactor data

Irradiation growth of zirconium alloys is a problem for operating power reactors primarily because of the distortions caused to fuel assemblies during operation. Distortion of the fuel assemblies results in interference between adjacent assemblies in PWRs, interference between fuel channels in BWRs, interference with reactivity control mechanisms in PWRs and control blades in BWRs. Irradiation growth is not the only cause of deformation leading to fuel assembly distortion; other factors (constraints, oxidation and hydrogen pick-up) are described in sections 2 and 4.

In the middle of the 1990's incomplete rod cluster control assembly (RCCA) insertions during emergency shutdown or during drop time tests had been reported by several PWR reactor operators in the world. The incomplete insertions were due to excessive deformation of fuel assemblies resulting in fuel assembly bow in either an "S" or "C" shape [Rudling et al., 2012]. Whereas bowing in some cases has been attributed to creep due to excessive hold-down forces, the cause of fuel assembly bow in other cases was attributed to abnormal axial growth of some parts of the fuel assembly components [Wilson et al., 1997]. WWER-1000 fuel assemblies have had similar issues to PWR assemblies, with assembly distortion and bow being a significant problem for both reactor types [Rudling et al., 2012].

BWR fuel elements are surrounded by Zircaloy-2 channel boxes that provide guidance to control blades, separate regions of coolant with differing states of flow and pressure, and provide structural strength and stiffness to the overall fuel assemblies. The channel boxes are designed to be used for more than one fuel assembly lifetime. They undergo deformations due to various material and mechanical interactions when residing in an operating BWR. Deformations such as bulge, bow and twist interfere with control blades and induce excessive moderation leading to localized power increases due to asymmetry of the water gap. The BWR fuel channel boxes operate at a positive internal pressure that causes outward creep deformation of the walls that is termed bulge. Channel bow is caused by neutron flux gradients and depends on the location and duration of exposure of the channel within the core. As a result of neutron flux gradients across fuel cells the fluence accumulated by a channel has an uneven planar distribution. Also, since irradiation growth depends on both material properties and fluence, BWR fuel channels also bow to accommodate the resulting uneven growth. Small variations in heat treatment, material composition, or texture tend to accentuate differential irradiation growth and fuel channel bow. The mechanisms of BWR channel deformation have been described in previous STRs on BWR fuel channel distortion [Garzarolli et al., 2011] and shadow corrosion-induced channel bow in BWRs [Rudling et al., 2012]. The effects of BWR channel distortion due to irradiation growth have also been reviewed by [Mader et al., 2011].

## 3.1.2    Materials test reactor data

Irradiation growth of Zr-alloys has been studied using nuclear reactors for over 50 years. Extensive R&D programs have been pursued, mostly in Russia, Europe and North America, and many of the results presented in journals and specialist conferences. Notable data include the work of: [Adamson, 1977] on the effect of cold-work increasing irradiation growth of Zircaloy-2; [Murgatroyd & Rogerson, 1984] showing breakaway (accelerated) irradiation growth in annealed Zircaloy-2; [Fidleris et al., 1987] showing how irradiation growth and breakaway growth varies in different alloys; [Rogerson, 1988a] showing breakaway growth in Zircaloys as a function of temperature; [Fidleris, 1988] showing the effect of temperature on irradiation growth for different alloys; [Shishov et al., 2004] showing irradiation growth behaviour of various Russian alloys in the BOR-60 reactor; and [Gilbon et al., 2000] showing differences between SRA and RXA Zircaloy material compared with M5 (PRXA) as part of the French R&D program.

Examination of neutron irradiated samples from the materials tested by Rogerson and Murgatroyd [Rogerson & Murgatroyd, 1983; Murgatroyd & Rogerson, 1984] showed that there was a correlation between accelerated growth and c-component dislocations [Holt & Gilbert, 1985], see Figure 3-1. The association between high strain rates and c-component dislocations has been a consistent element of all subsequent studies of irradiation growth.
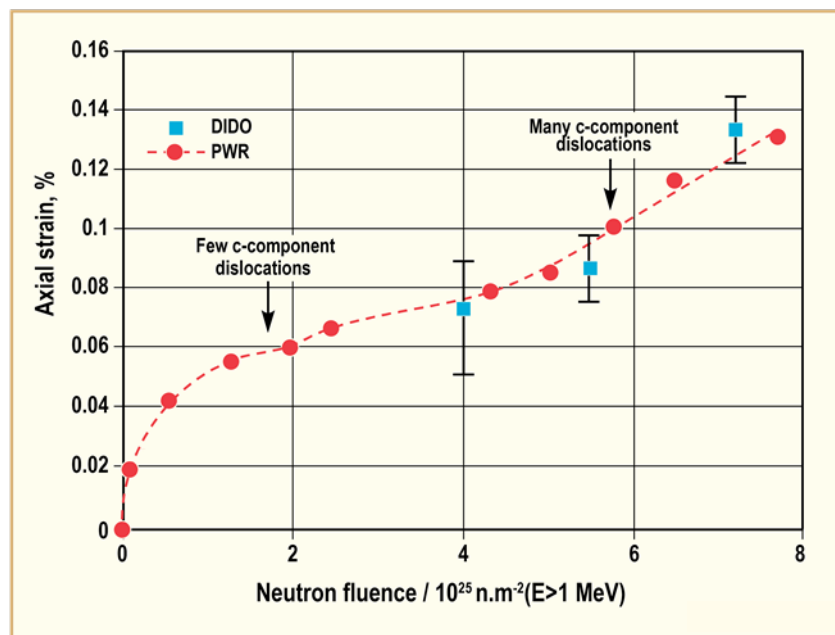


Figure 3-1:     Irradiation growth in annealed (RXA) Zircaloy at 550 K –580 K, showing accelerating growth after a fluence of about 4 x 10$^{25}$ nm$^{-2}$ (E>1 MeV). Adapted from [Holt & Gilbert, 1985] and [Fidleris, 1988].

The nature of the c-component dislocations responsible for accelerated, or breakaway, growth is discussed in detail in Section 3.3.2.2.2. For now it is sufficient to say that the high rates of irradiation growth are associated with the presence of c-component dislocations that are produced by cold-working or evolve during irradiation [Holt et al., 1982; Holt & Gilbert, 1986]. Subsequent analysis of the materials exhibiting breakaway growth (corresponding with the data shown in Figure 3-1) showed that the c-component dislocations created by irradiation were extended defects (stacking-faults) on the basal plane and were vacancy in nature [Griffiths & Gilbert, 1987]. These extended defects were created by a net flux of vacancy point defects resulting in climb on existing network c-component dislocations in cold-worked material, or by the nucleation of discrete c-component dislocation loops in annealed materials. Although climb of c-component network dislocations, or point defect clustering, on non-basal planes is observed in certain circumstances [Griffiths & Gilbert, 1987; Griffiths et al., 1987; Griffiths, 1988; Griffiths et al., 1989; Griffiths et al., 1993], it is the climb of extended vacancy defects on the basal plane that is coincidental with accelerated or breakaway growth [Griffiths &Gilbert, 1987; Griffiths et al., 1989; Griffiths et al., 1995]. Early evidence indicated that

the stability of c-component dislocation loops responsible for accelerated breakaway growth was affected by impurities [Griffiths & Gilbert, 1987; Griffiths et al., 1989], consistent with the earlier findings of Jostsons et al. [Jostsons et al., 1977; Jostsons et al., 1979] linking vacancy, basal plane, dislocation loop formation in neutron irradiated Zr with the effect of an unidentified interstitial impurity or impurities.

Impurity effects aside, the differences in irradiation growth for different engineering alloys studied as part of the Russian R&D program have been summarised by [Shishov et al., 2004]. The Russian work compared Zircaloy-2 and Zircaloy-4 with Russian alloys, E110, E125 and E635, irradiated at temperatures between 295°C and 350°C (Figure 3-2). Similarly, other alloys studied as part of the French R&D program (Zircaloy-2 and -4, M4 and M5) have been compared by [Gilbon et al., 2000], Figure 3-3. A joint program between Canada and the US compared the growth behaviour of alloys developed in Canada and the US [Tucker et al., 1984]. The latter study included Zircaloy-2, Zircaloy-4, Zr-2.5Nb, Excel, sponge Zr and crystal-bar Zr (Figure 3-4). Research in the UK was primarily directed at Zircaloy-2, addressing the effects of cold-working and temperature and was summarised by [Rogerson, 1988a], reproduced in Figure 3-5, and [Fidleris,1988], reproduced in Figure 3-6.

In all cases where post-irradiation examinations were performed, high growth rates were shown to correlate with the observation of c-component dislocations. For cold-worked materials the growth rate was correlated with c-component dislocation density (specifically the ratio of c and a-dislocation densities [Griffiths et al., 1989]) and, for annealed materials, accelerated (breakaway) growth coincided with the formation of discrete basal plane dislocation loops [Griffiths & Gilbert, 1987]. The results described by [Adamson, 1977], and [Rogerson, 1988a], showing increased growth with cold-working, are at odds with the Russian results comparing irradiation growth of 40% cold-worked and recrystallised E635 alloy [Shishov et al., 2005]. In the latter study there was no difference in growth behaviour between annealed E635 and the same material cold-worked by 40%. The lack of increased irradiation growth in the cold-worked material was attributed to the effect of the alloying elements (Sn and Nb) in delaying breakaway growth [Shishov et al., 2005]. This conclusion presumed that breakaway growth (accelerated growth after an incubation period) occurred in both annealed and cold-worked material even though the breakaway effect (involving an incubation period of low growth) was limited to annealed materials [Fidleris, 1988]. The explanation for the low growth rates observed in cold-worked E635 alloy given by [Shishov et al., 2005] was not consistent with other data showing that the rate of growth was correlated with the density of c-component dislocations, whether from cold-working or from dislocation loop formation [Holt et al., 1982; Griffiths et al., 1989]. The Russian results may be reconciled with other data if recrystallisation of the cold-worked material occurred during the irradiation because of the high irradiation temperature (330°C - 360°C). Some support for this possibility comes from the statement made in the original Russian report comparing the annealed and cold-worked E635 results [Nikulina et al., 1999], in which it was stated that, with reference to E635, "The irradiated materials were fully recrystallised, regardless of their different initial states (recrystallised or cold-worked)".

Cold-working aside, the Russian results [Shishov et al., 2005] indicated that E635, an alloy containing Zr-1Nb-1.3Sn-0.4Fe, similar to Zirlo (Zr-1Nb-1Sn-0.1Fe), exhibited the lowest irradiation growth compared with other alloys tested under the same conditions. [Shishov et al., 2005] tested various combinations of Zr-Nb, i.e. Zr –1Nb and Zr-2.5Nb, Zr-Sn-Fe-Cr(Ni) (similar to Zircaloy-2 and Zircaloy-4) and Zr-Sn-Nb-Fe (variants close to the composition of E635, ZIRLO and NSF). They concluded that, "E635 type alloys have the longest incubation period prior to the [onset of] accelerated growth that is practically independent of the structure state (CW or recrystallization annealed in the α- and (α + β)- regions)". Very little data are available concerning materials reactor tests on Zirlo developed by Westinghouse (Zr-1Sn-1Nb-0.1Fe). Results for an alloy similar to Zirlo and E635, i.e. NSF developed by GE, have been obtained that corroborate the Russian results indicating that alloys based on Zr, Sn and Nb exhibit the lowest irradiation growth rates [Kobylyansky et al., 2007]. The Russian data suggested that Nb alone is not as effective in suppressing accelerated irradiation growth as the combination of Sn and Nb because E110, an alloy similar to M5 and based on Zr-1Nb, exhibited high growth rates relative to E635 irradiated under the same conditions [Shishov et al., 2005]. The high rate of growth of E110, in this instance, may be the result of high hydrogen pick-up or low Fe content (see Section 2). Whereas numerous results point to the role of Fe in reducing irradiation growth (see Section 2), Kobylyansky et al. concluded that "From the viewpoint of suppression of irradiation-induced growth in zirconium materials, the positive effect of iron is

revealed only in its joint action with niobium or tin" [Kobylyansky et al., 2007]. The role of Fe as a suppressor (or promoter) of c-component loop formation may then depend on whether one is examining unalloyed Zr, or Zr alloyed with Sn and/or Nb (see Section 3.3.1.4.1).

In the work of [Shishov et al., 2005] a synergistic effect of Sn and Nb in suppressing c-component loop formation was implied. Shishov et al. made observations on beta-quenched materials where it was claimed that α-grains, containing Sn and Nb in solid solution, had few c-component loops after irradiation whereas α'-grains, containing Sn only, contained many c-component loops after irradiation. A further synergy with Fe was also apparent. Shishov et al., reported that the growth rate of E635 increased to match that of E110 by reducing the Fe content in E635 from 0.35wt% to 0.15wt% (Figure 3-7). The role of Fe in suppressing c-component loop formation is at odds with the earlier studies showing that basal plane c-component loops were more prevalent in impure materials if one considers that Fe acts the same as other interstitial impurities in affecting c-component loop formation. It may be that Fe does not affect Zr in the same way as other interstitial impurities, or that the Fe does not suppress c-component loop formation in unalloyed Zr, as concluded by [Kobylyansky et al., 2007]. Even though there is evidence that Fe segregates at vacancy loops (see Section 3.3.1.4.1), the Russian results indicate that this segregation is probably an effect rather than a cause of basal plane vacancy loop formation. The Russian results also indicate that E110 is more susceptible to breakaway growth compared with annealed Zircaloy-2 or -4, having a shorter incubation period before breakaway growth (Figure 3-7). The Russian data for E110 shown in Figure 3-2 and Figure 3-7 are at odds with the French data for the comparable alloy, M5, shown in Figure 3-3. The difference in growth behaviour was attributed to differences in the onset of breakaway growth due to differences in minor impurity/alloying additions such as Fe and O in E110 compared with M5 [Shishov et al., 2005]. The Fe content of M5 is nominally 400 wtppm (Table 2-6), which is similar to that for optimised E110 (Table 2-10), but other factors, such as hydrogen pick-up, may also play a role (see Section 2).

It is clear that alloys containing only Sn in the matrix exhibit the highest rates of irradiation growth and those alloys containing both Nb and Sn exhibit the lowest irradiation growth. It is not just a simple case of adding Nb to the alloy, however. Excel alloy, developed in Canada, is similar to Zirlo and E635 in that it contains both Nb and Sn plus other impurity/alloying elements that form second phases (Fe, Cr and Ni). There are other impurities such as Si, C, O and N but the evidence indicates that it is the absence of Nb from the alpha-phase solid solution that is mainly responsible for the very high rates of irradiation growth in Excel compared to other Nb-containing alloys [Griffiths et al., 1987; Giffiths et al., 1989]. The reason is that Excel contains 3.5 wt% Sn, as compared with 1 wt% Sn in both Zirlo and E635. As a result of the high Sn content in Excel alloy the Nb resides exclusively in the beta-phase with the alpha phase containing Sn only in solid solution. In both Zirlo and E635 the alpha phase contains Nb in solid solution together with the Sn. The observations of high rates of accelerated growth and high densities of c-component loops in the irradiated Excel alloy [Griffiths et al., 1989] is consistent with the observations on quenched E635 alloy following irradiation [Shishov et al., 2005] where it was claimed that α'-grains, containing Sn and Nb in solid solution, contained fewer c-component loops compared with α-grains containing Sn in solid solution only. The effect of increasing the Fe content in reducing the irradiation growth in Zr-Sn-Nb-Fe alloys is enigmatic because, from the Russian results [Shishov et al., 2005; Kobylyansky et al., 2007], it would appear that it is the synergistic effect of Fe combined with Sn and/or Nb in solid solution that is important in suppressing c-component loop formation and growth. The possible mechanisms by which increased Fe content reduces irradiation growth are discussed in Section 3.3.1.4.1.

The results of [Shishov et al., 2005] concerning the Zr-1Nb alloy, E110, were ambiguous in terms of the role of Nb on irradiation growth because Zr-1Nb (E110) alloy exhibited high rates of irradiation growth (Figure 3-2 and Figure 3-7). Hydrogen pick-up aside the effect of Nb alone on irradiation growth is confounded by the fact that the E110 had a low Fe content and therefore it is not clear whether it is the low Fe content that resulted in high growth rates observed in E110 compared with E635. A more recent study by [Yagnik et al., 2016], showed that, for a given Fe content, both Zr-1Nb and Zr-1Sn-1Nb exhibited lower irradiation growth compared with Zr-1Sn. Yagnik's results indicate that Nb + Sn is just as effective in limiting growth as Nb alone (in M5 and Zr-2.5Nb alloys at least). Given that Zr-Sn alloys exhibit the highest rates of irradiation growth, it is not clear how Nb, either alone in Zr-Nb alloys or in conjunction with Sn in Zr-Sn-Nb alloys, affects the irradiation growth.

There are some indications from electron irradiation [Griffiths et al., 1993] that the propensity for c-loop formation decreases with the presence of Nb. A strong effect of Nb was observed in studies of loop growth kinetics during electron irradiation by [Buckley & Manthorpe, 1980]. In another study by [Buckley et al., 1980], it was shown that adding Sn increases loop densities and reduces loop growth rates. In the latter case analysis of loop growth data indicated that the binding energy between the vacancy and the Sn atom was about 0.3 eV. This increase in binding energy effectively increases the vacancy migration energy when the solute is a slow diffuser, as is the case for Sn [Hood, 1988]. The observations that both Sn and Nb increase a-type loop densities and slow a-type loop growth rates is consistent with the theoretical results of [Christensen et al., 2016], in particular with respect to the effect of Nb.

The most rigorous, controlled, irradiation growth study to date has been conducted by [Yagnik et al., 2016]. That study was directed at specific variables known, or suspected, to influence irradiation growth. As much as possible all microstructure and chemistry variables were minimised except for the variable of interest, in particular Fe, H and cold-work. The most noteworthy results are summarised:

1. [Yagnik et al., 2016] studied the effect of Fe on irradiation growth for Zr-1Sn, Zr-1Nb-1Sn and Zr-1Nb base alloys. Zr-1Sn is representative of the response expected for Zircaloy-2 and -4; Zr-1Nb-1Sn is representative of the response expected for Zirlo and E-635 alloys; and Zr-1Nb is representative of the response expected for M5, E110 and Zr-2.5Nb /E125 alloys. [Yagnik et al., 2016] showed that increasing the Fe content reduced irradiation growth for all alloy types (see Figure 2-60, Section 2).The results of this Fe variability study also showed that irradiation growth decreased in the order Zr-1Sn>Zr-1Nb>Zr-1Nb-1Sn for Fe concentrations >1000 wtppm and Zr-1Sn>Zr-1Nb-1Sn>Zr-1Nb for Fe concentrations <1000 wtppm.

2. The effect of H was investigated and it was shown that H increased irradiation growth (see Figure 2-80, Section 2). Although it is not clear how the H enhances the growth, whether through the effect of H in solid solution or as hydrides, it is known that H enhances self-diffusion by reducing vacancy formation energies [Iida et al., 2005].

3. There is only a weak dependence of irradiation growth on cold-work up to levels of 20% cold-work for Zircaloy-2, E635 and NSF alloys as reported by [Kobylyansky et al., 2010], see Figure 2-14, Section 2. Similar results were also shown by [Yagnik et al., 2016] for Ziracloy-2 and NSF alloys cold-worked up to 20%. In the study of [Yagnik et al., 2016], Zircaloy-2 material cold-worked to 70% deformation exhibited high, linear rates of irradiation growth from low doses but these rates were less than that of post-breakaway annealed material after a fluence of 5 x $10^{25}$ n.m$^{-2}$ (see Figure 2-13 and 2-29, Section 2 [Yagnik et al., 2016]. The results on cold-working can be understood if the low levels of cold-work, in the work reported by [Kobylyansky et al., 2010] and [Yagnik et al., 2016], introduced mainly a-type dislocations at levels <20% cold-work, with an increasing proportion of c-type dislocations with higher levels of cold-work (see Section 3.3.2.1.2). This is conceivable depending on the Schmid factors for prismatic a-slip and pyramidal <c+a> slip when the material is deformed. The Schmid factors are dependent on the mode of deformation and the texture. It is well known that the critical resolved shear stress for c-component slip is higher than for a-slip. One can expect more c-component slip with increasing cold-work as the material hardens. If the deformation mode is such that the easy a-slip systems are activated, then c-slip would not occur until the material had work-hardened at higher levels of cold-work. The results of [Yagnik et al., 2016] can be reconciled with previous work if one assumes that the c-component dislocation density is not increasing as much as the a-type dislocation density between 0% and 20% cold-work (section 3.4,). In section 3.3.2.1.2 the data on irradiation growth rates in Zircaloy-2 at 330 K [Fidleris et al., 1987; Griffiths et al., 1989] have been re-assessed. The data show a linear increase in irradiation growth rate with ratio of c-type and a-type dislocations, in keeping with the expectations based on rate theory (section 3.4). It is noteworthy that the data of [Yagnik et al., 2016] also show that the rate of growth (per unit dpa) was higher for annealed material exhibiting accelerated breakaway growth compared with cold-worked material, i.e. the post-breakaway growth rate is higher than the linear rate exhibited by the 70% cold-worked material. This can also be understood in terms of the relative proportion of c- and a-component dislocations (section 3.4).
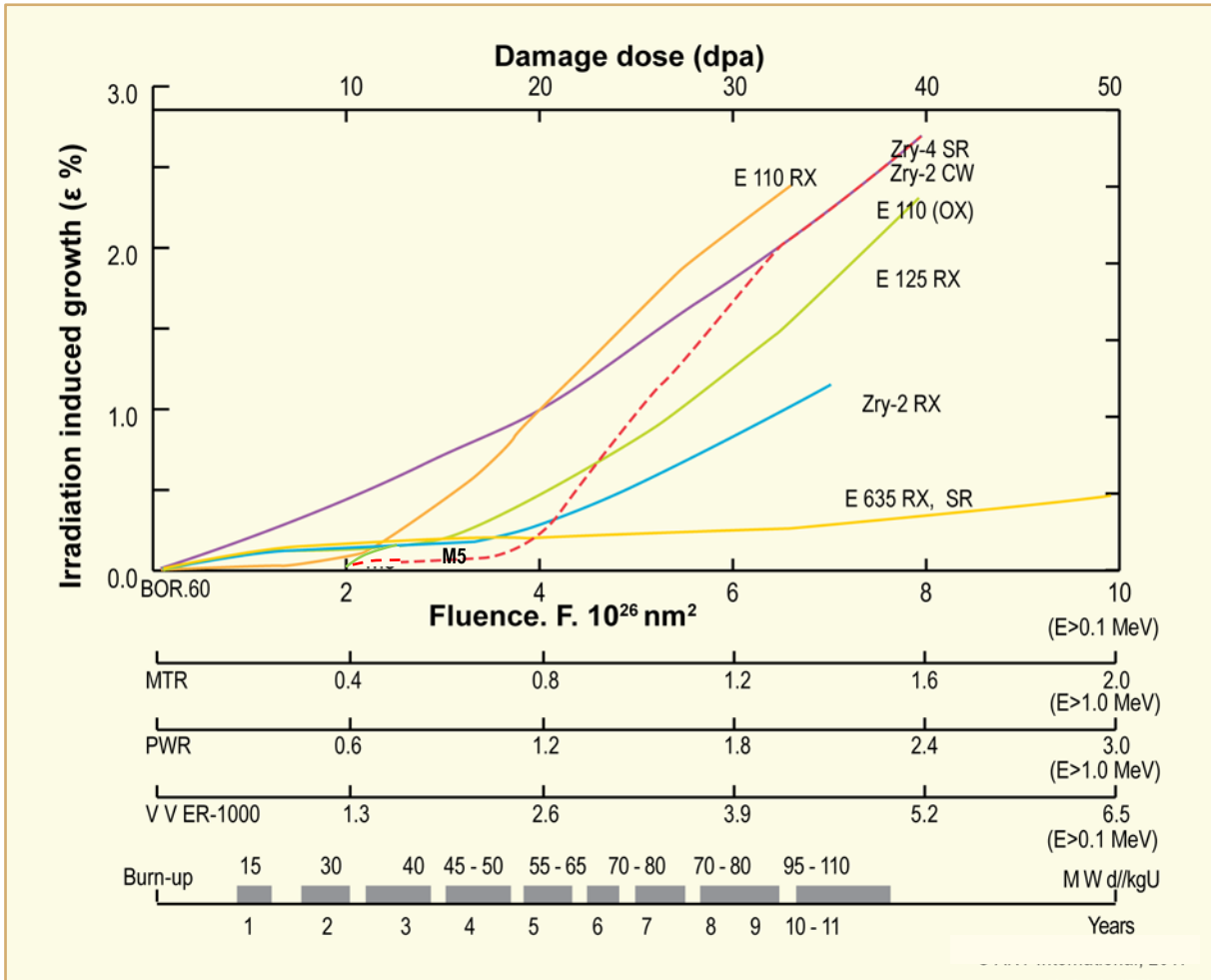
Figure 3-2:     Irradiation growth of Zr alloys at 290 °C –350°C as a function of neutron fluence and damage dose, [Shishov et al., 2005]. The E110(OX), represented by the red dashed line, refers to E110 RX (recrystallized) material that had an oxide pre-treatment prior to irradiation to minimize hydrogen pick-up during irradiation.
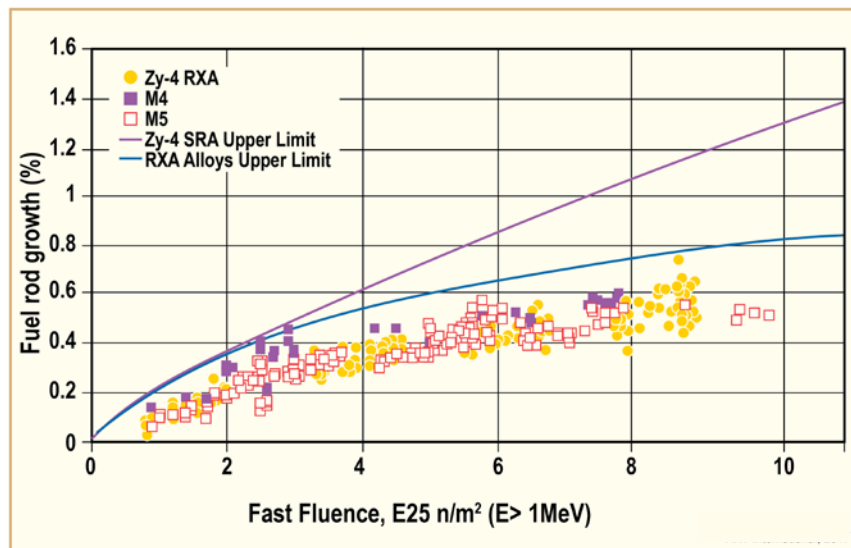


Figure 3-3:     Irradiation growth of Zr alloys at about 300°C as a function of neutron fluence and damage dose. Adapted from [Gilbon et al., 2000].

# 4 Engineering applications - Charles Patterson

## 4.1 Introduction and overview

The deformation mechanisms and factors that contribute to irradiation growth are reviewed in Section 1 through Section 3. Growth models based of varying degrees of detail are also described. The significant points relative to engineering applications are that strains due to irradiation growth depend on

- Material composition, including impurities (e.g., hydrogen),

- Crystallographic texture (anisotropy),

- Microstructure (dislocation density, grain size and shape),

- Fabrication and heat treatment processes (residual stress),

- Fast neutron flux and time (fluence, due to high energy neutrons)[4],

- Temperature

and

- Time.

This section reviews the practical effects of irradiation growth on the performance of zirconium alloys and the manner in which these effects are addressed in the design and operation of water reactor fuel.

As a point of general background, the issue of irradiation growth is essential to reactor safety. The distortion of components such as fuel rods, water rods, guide tubes, fuel assemblies and BWR channels due to the combined effects of applied mechanical loading, creep, in-reactor corrosion, hydriding and irradiation growth can affect fundamental safety requirements for fuel coolability, reactivity control and, in the case of the CANada Deuterium Uranium (CANDU) and other pressure tube reactors, the integrity of the primary pressure system. Coolability issues have been observed to arise when deformation mechanisms affect coolant flow, heat transfer and critical heat flux; e.g., the departure from nucleate boiling (DNB) in PWRs or the critical heat flux (CHF) in BWRs and PHWRs. Reactivity issues arise when fuel assemblies are distorted to the extent that local power peaking occurs in regions of large water gaps or when the lateral distortion is sufficient to impede or prevent the insertion of control rods when their use is required.

Irradiation growth poses potential performance issues for zirconium-based components that are physically large (long) and that are exposed to large fast neutron fluence at temperatures in the range of current, water-reactor nuclear power plants. Issues associated with irradiation growth of zirconium alloys were recognized early in the naval and civilian nuclear reactor programs, [Buckley, 1961]. Irradiation growth which was observed in the pressure tubes of early CANDU reactors and the N-reactor[5] led to a large amount of research and development related to the mechanisms and conditions for dimensional changes. Growth was also observed in early power-producing LWRs and became a greater factor in the design and operation of fuel and zirconium-based components as burnup and in-core residence time increased.

---

[4] Damage is observed in zirconium at neutron energy levels above a threshold of about 25 eV, but is commonly assessed relative to energy levels >1 MeV.  E > 1 MeV is assumed throughout this section.

[5] The N-Reactor was a water/graphite-moderated nuclear reactor operated by the U.S. government at the Hanford Site in Washington. It was designed to produce weapons-grade plutonium and electrical power. Plutonium production began in 1963. Electrical production began in 1966. The reactor was shut down in 1987, placed on cold standby in 1988 and deactivated between1994 and 1998.

As noted in prior sections, irradiation growth and the distortion of affected components are mitigated by means of a varying combinations of design, material selection and operational practices. These aspects are reviewed in this section from the perspective of the methods and materials that are commonly used in design and licensing. Section 4.2 reviews engineering models and presents growth correlations for common fuel rod cladding materials. Section 4.3 assesses the magnitude of strains due to irradiation growth and other deformation mechanisms relevant to fuel rods and assembly structural components. Section 4.4 reviews the methods used to mitigate or eliminate the effects of irradiation growth. Section 4.5 presents a brief summary and discussion of this information.

## 4.2 Engineering models

### 4.2.1 Growth correlations

Previous sections of this report describe current understandings regarding the irradiation growth of Zr-alloys in terms of observed behaviour, growth mechanisms and phenomenological explanations of the growth process. This information has provided the bases for the development of growth resistant materials and fabrication processes. It also has provided the basis for analytic models of varying degrees of complexity that range from correlations based on observed behaviour to phenomenological models based on fundamental mechanisms of irradiation growth as discussed in Section 3.

While the fundamental understandings noted previously have contributed to the development of materials and their methods of fabrication, models based on first principles tend not to be used in engineering applications. Instead, design and licensing analyses typically utilize empirical correlations that are based on observations of the effects of irradiation on a material and, frequently, on specific components in the relevant operating environments. That is, separate correlations are commonly developed for each material type and heat treatment based on the observed, in-reactor behaviour of components or samples representative of fuel cladding, guide tubes, spacer/grid strip or sheet. One of the motivations for the use of models that are empirically based or that are phenomenological but based on a large number of in-reactor measurements is the need to identify the uncertainty in model predictions relative to safety limits; i.e., prediction uncertainties are more readily accepted in the design and licensing arenas when a model is based directly on the a large number of observations of the effects of in-reactor operation rather than on a set of postulates and a limited amount of experimental data.

The empirical correlations for the irradiation growth of zirconium alloys utilized in design and licensing analyses are generally of a power-law form given by (see [Geelhood et al., 2015] and [Luscher et al., 2015] for a working example):

Equation 4-1:
$$\Delta \boldsymbol{\varepsilon}^{ir} = A^{ir} \mathbf{G} \left( \phi_t \Delta t \right)^m$$

in which

$\Delta \boldsymbol{\varepsilon}^{ir}$ = Vector of incremental of irradiation growth strains over time interval $\Delta t$,

$A^{ir}$ = Growth rate coefficient,

$\phi_t$ = Neutron flux during time interval $\Delta t$, generally with E > 1 MeV

and

m = Growth exponent.

The effect of material texture is approximated in Equation 4-1 by the vector

Equation 4-2:
$$\mathbf{G} \simeq \mathbf{1} - 3\mathbf{f}$$

in which the vector $\mathbf{f}$ consists of the Kearns texture factors in the principal material directions; e.g.,

Equation 4-3:
$$\mathbf{f} = \left\{ \begin{array}{c} f_n \\ f_t \\ f_l \end{array} \right\} = \left\{ \begin{array}{c} f_r \\ f_d \\ f_a \end{array} \right\}$$

in which $n$ is normal to the plane of rolling, $t$ is in the rolling plane and transverse (normal) to the rolling direction and $l$ is in the rolling plane and in the longitudinal rolling direction for planar materials. The subscripts $r$, $d$ and $a$ are the corresponding radial, diametral and axial directions for tubular products. For reference, typical texture factors are given in Table 4-1. The texture difference between cladding and pressure tubes is a deliberate artifact of the respective manufacturing processes; i.e., pilgering for cladding versus hot extrusion followed by drawing for pressure tubes.

Table 4-1: Typical texture factors for zirconium-alloy tubular and sheet components; [Adamson & Rudling, 2001], [Holt et al., 2000].

| Material Direction | Cladding Guide Tubes Water Rod | Pressure Tubes | Rolled Sheet |
|---|---|---|---|
| fn (fr) | 0.60 | 0.32 | 0.60 |
| ft (fd) | 0.33 | 0.62 | 0.30 |
| fl (fa) | 0.07 | 0.06 | 0.20 |
| | | | © ANT International, 2017 |

The strain due to irradiation growth is typically determined by numerical integration of Equation 4-1 with respect to fast neutron flux and time because flux varies during the course of irradiation; i.e.,

Equation 4-4:
$$\varepsilon^{ir}_{t+\Delta t} = \varepsilon^{ir}_t + \Delta\varepsilon^{ir}.$$

In LWR fuel, a primary concern is the elongation of cladding, guide tubes and fuel channels, so growth strain is computed in the axial direction according to

Equation 4-5:
$$\left( \frac{\Delta L}{L} \right)^{ir}_{t+\Delta t} = \left( \frac{\Delta L}{L} \right)^{ir}_t + A^{ir}_l \left( \phi_t \Delta t \right)^m$$

In Equation 4-1 and Equation 4-5, the growth coefficient, $A^{ir}$, and exponent, $m$, are empirical terms which depend on factors such as material composition, texture, grain size and shape, dislocation density (heat treatment) and operating conditions (temperature). For reference, the values used with Equation 4-5 in the referee code of U.S. NRC (FRAPCON-4.0) are listed in Table 4-2. Fuel suppliers use proprietary relationships that are either similar to Equation 4-1 or Equation 4-5 or that address more of the phenomena that affect irradiation growth as discussed in prior sections of this report as discussed in the earlier sections of this report.

Table 4-2: Coefficients in model for irradiation growth of fuel cladding in the longitudinal direction from FRAPCON-4.0 code, [Luscher et al., 2015].

| Material | A ir | m | Notes |
|---|---|---|---|
| Zry-2 RXA | 1.0900E-21 | 0.8450 | Assumed to be 50% of Zry-4 RXA |
| Zry-2 RXA | 2.6639E-20 | 0.8684 | Fit of data from [Luscher et al., 2015] |
| Zry-4 SRA | 2.1800E-21 | 0.8450 | |
| M5 | 7.0130E-21 | 0.8179 | |
| ZIRLO | 9.7893E-25 | 0.9824 | |
| Opt. ZIRLO | 9.7893E-25 | 0.9824 | Assumed to be the same as ZIRLO |
| | | | © ANT International, 2017 |

Examples of irradiation growth models for Zry-2 (RXA), Zry-4 (SRA), M5 (RXA) and ZIRLO fuel cladding are shown in Figure 4-1 through Figure 4-4 along with the supporting data. These plots are based on the irradiation growth model in the FRAPCON code (Equation 4-5) with the growth coefficients and fluence exponents listed in Table 4-2. The references to data in these figures are given by [Luscher et al., 2015]. The upper 95% and lower 5% confidence and prediction limits were determined by re-fitting the respective data as $\log(\varepsilon^{ir})$ relative to $\log(\phi t)$ and are included for reference. Note that basing the FRAPCON growth models on measurements of fuel cladding elongation biases the resulting calculations to values greater than elongation due to irradiation growth alone. This issue is discussed briefly later in this section.
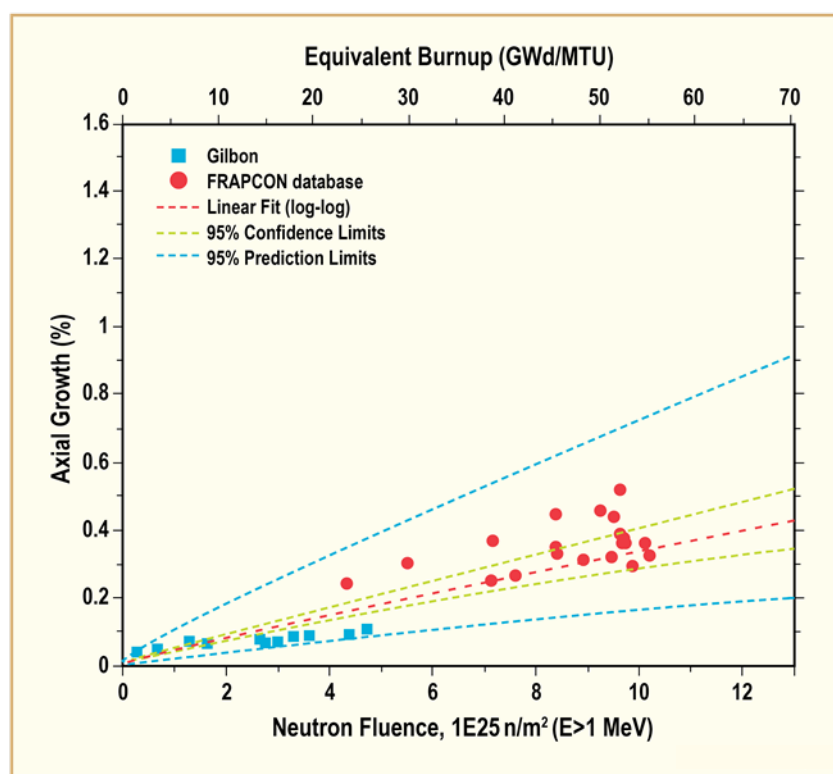


Figure 4-1: Irradiation growth of RXA Zry-2 fuel cladding relative to neutron fluence; fit of data used by [Luscher et al., 2015].
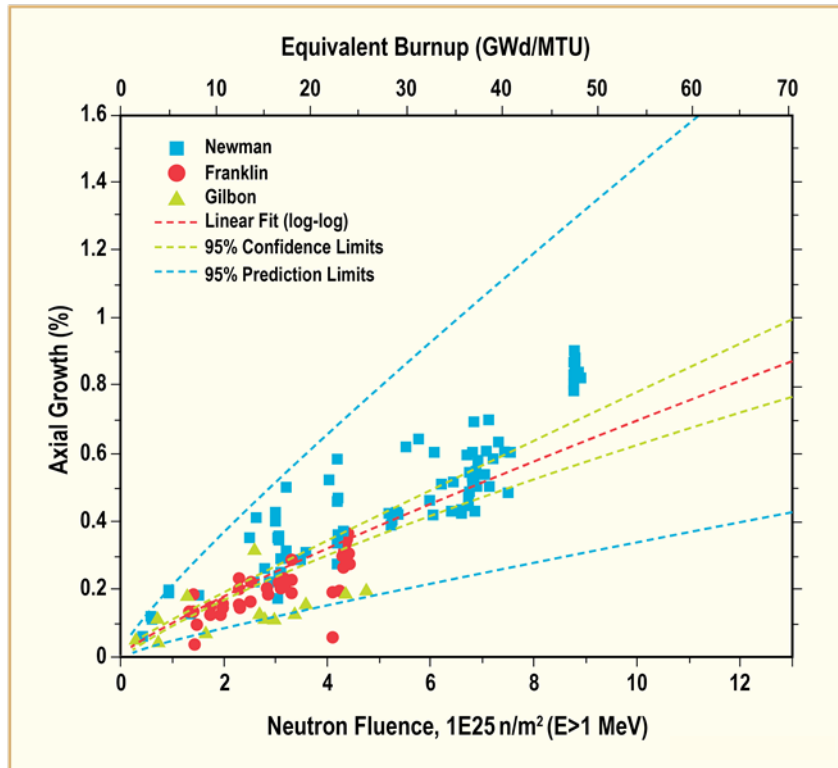
Figure 4-2: Irradiation growth of SRA Zry-4 fuel cladding relative to neutron fluence, data of [Luscher et al., 2015].
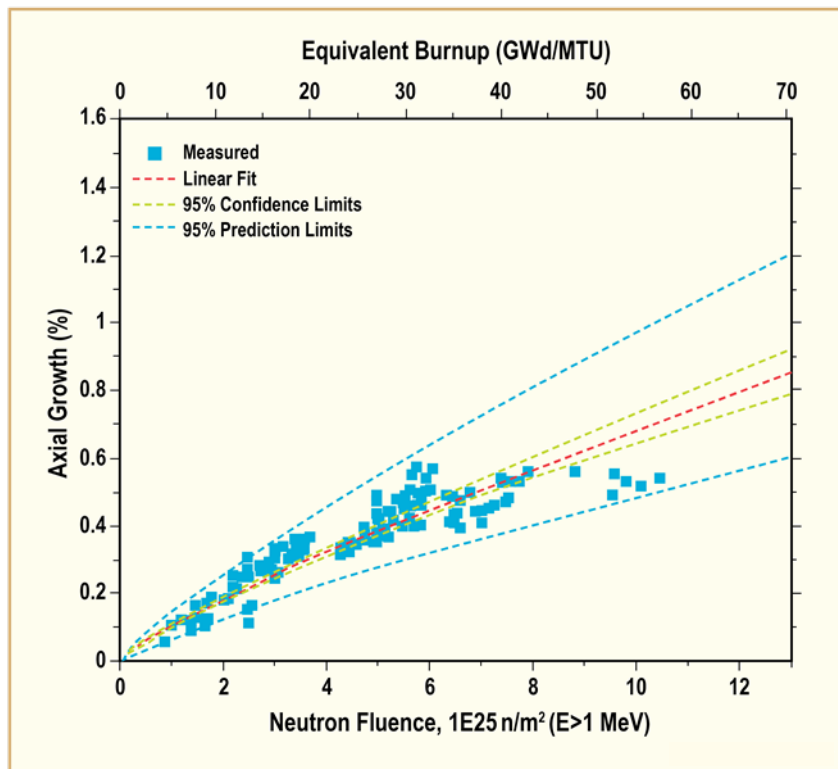


Figure 4-3: Irradiation growth of RXA M5 fuel cladding relative to neutron fluence, data of [Luscher et al., 2015].
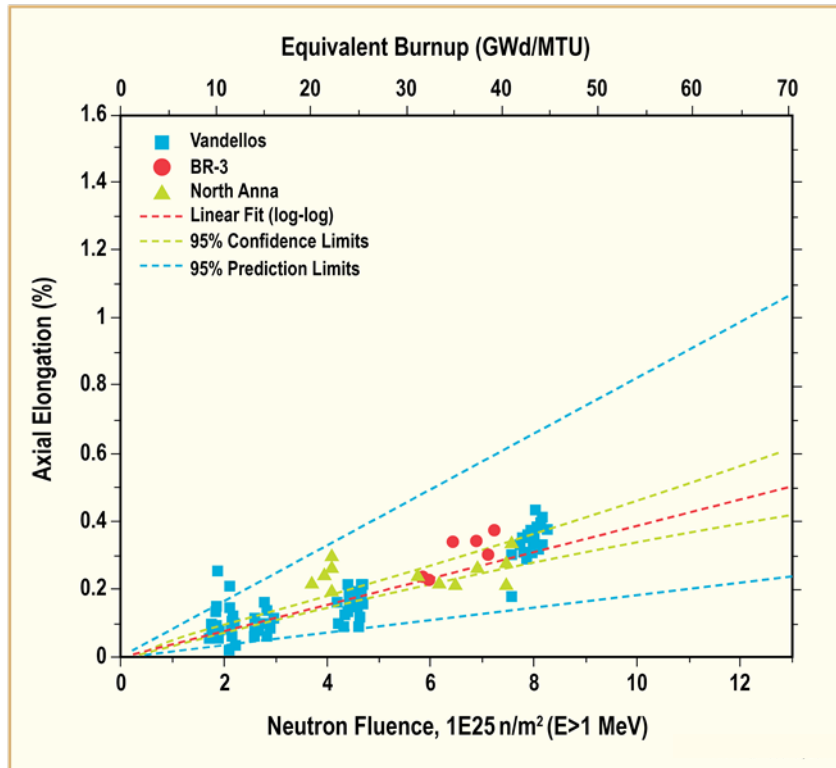
Figure 4-4:    Irradiation growth of ZIRLO fuel cladding relative to neutron fluence, data of [Luscher et al., 2015].

The reliance on unique fitting terms for each material and heat treatment implicitly factors the effects of dislocation density, grain size, and cold work into the power-law relationships of Equation 4-1 and Equation 4-5. Although these factors were shown to affect irradiation growth in Section 2 and Section 3, engineering growth correlations are generally developed for a particular material and fabrication process. As a result, the applications of power-law models like Equation 4-1 are limited to the conditions and ranges of data on which they are based.

Temperature is a factor that is addressed only indirectly in growth models like Equation 4-1 and Equation 4-5 that utilize fixed fitting terms. The growth coefficient and fluence exponent are derived empirically from measurements at temperatures representative of the intended application. As shown in previous sections of this report, temperature affects irradiation growth in a nonlinear manner that varies with both temperature and neutron fluence; see Figure 4-5, which is repeated below from an earlier section for convenience. But the rate of growth in the saturated, low-growth regime varies only slightly within the range of temperatures at which water reactor fuel typically operates. For example, the relative change in growth strain rate is less than 0.2%/K at temperatures below 340-350°C (610-620 K) based on growth rate assessments by [Fidleris et al., 1987] shown in Figure 4-6. This variation is small when compared to the uncertainties of Equation 4-1 as indicated by the prediction intervals of Figure 4-1 through Figure 4-4. As a result, the growth model in FRAPCON is applied at temperatures up to 360°C without adjustment for temperature.

Note, however, that the rate of irradiation growth varies by a larger amount than indicated above when considered over the full range of possible temperatures, particularly above 340-360°C. This condition leads to variants of Equation 4-1 by fuel suppliers in which the empirical terms, $A^{ir}$ and $m$, are expanded to include the effects of temperature or are varied in a stepwise manner with temperature. An example of such a variant is the irradiation growth model for Zr-2.5Nb pressure tubes described by Causey et al. [2000], viz.,

Equation 4-6:    $$\Delta \varepsilon_i^{ir} = A^{ir} G_i \exp\left( -\frac{Q^{ir}}{T} \right) \phi \, \Delta t$$

# References

Adamson R. B., *Cyclic Deformation of Neutron Irradiated Copper*, Phil. Mag. 17, pp. 681, 1968.

Adamson R. B., *Irradiation Embrittlement and Creep in Fuel Cladding and Core Components*, Proceedings of BNES Conference, p. 305, London, 1972.

Adamson R. B., *Irradiation Growth of Zircaloy,* Zirconium in the Nuclear Industry; Third Conference, ASTM STP 633, p. 326, 1977.

Adamson R. B., Tucker R. P. and Fidleris V., *High-Temperature Irradiation Growth in Zircaloy,* Zirconium in the Nuclear Industry, 5th Conference, ASTM STP 754, D. G. Franklin, Ed., American Society for Testing and Materials, 208-234, 1982.

Adamson R. B. and Bell W. L., *Effects of Neutron Irradiation and Oxygen Content on the Microstructure and Mechanical Properties of Zircaloy, Microstructure and Mechanical Behaviour of Materials*, Proceedings: Int'l Symposiums, Xian, China, October 1985, EMAS, pp. 237-246, Warley, UK, 1986.

Adamson R. B., *Effects of Neutron Irradiation on Microstructure and Properties of Zircaloy*, Zirconium in the Nuclear Industry; Twelfth International Symposium, ASTM STP 1354, pp. 15-31, West Conshohocken, PA, 2000.

Adamson R. B. and Rudling P., *Mechanical Properties of Zirconium Alloys*, ZIRAT6/IZNA1 Special Topics Report, ANT International, Mölnlycke, Sweden, 2001/2002.

Adamson R. B., Cox B., Strasser A., Rudling P., *ZIRAT6/IZNA1 Annual Report*, ANT International, Mölnlycke, Sweden, 2001/2002.

Adamson R. B. and Rudling P., *Dimensional Stability of Zirconium Alloys*, ZIRAT7/IZNA2 Special Topics Report, ANT International, Mölnlycke, Sweden, 2002/2003.

Adamson R. B., *Recovery of Irradiation Damage by Posts-Irradiation Thermal Annealing-Relevance to Hydrogen Solubility and Dry Storage Issues*, EPRI Technical Report 1013446, June 2006.

Adamson R. et al., *Corrosion Mechanism in Zirconium Alloys*, ZIRAT12, Advanced Nuclear Technology International, Skultuna, Sweden, 2007.

Adamson R. B. et al., ZIRAT14/IZNA9 Annual Report, ANT International, Mölnlycke, Sweden, 2009.

Adamson R. B, Garzarolli F. and Patterson C., *In-Reactor Creep of Zirconium Alloys*, ZIRAT14/IZNA9 Special Topical Report, ANT International, Mölnlycke, Sweden, 2009a

Adamson R. B., *Zirconium Production and Technology: The Kroll Medal Papers* 1975-2010, ASTM RPS2, ASTM I, West Conshohocken, PA, 2010.

Adamson R. B. et al., *ZIRAT15/IZNA10 Annual Report*, ANT International, Mölnlycke, Sweden, 2010.

Adamson R. et al., *ZIRAT16/IZNA11 Annual Report,* ANT International, Mölnlycke, Sweden, 2011.

Adamson et al., *ZIRAT21/IZNA16 Annual Report*, ANT International, Mölnlycke, Sweden, 2016.

Aitchison et al., *The Thermal Cycling of Zirconium*, in Proc. of Int. Conf. on Properties of Reactor materials and the Effects of Radiation damage, Berkeley, UK, pp. 431-439, 1961.

Alexander W. K., Fidleris V. and Holt R. A., *Zry-2 Pressure Tube elongation at the Hanford N Reactor*, ASTM Spec. Techn. Publ. 633), pp. 344-364, 1977.

ASTM Standard E263-09, *Standard Test Method for Measuring Fast-Neutron Reaction Rates by Radio-activation of Iron.*

Andersson T., Almberger J. and Björnkvist L., *A Decade of Assembly Bow Management at Ringhals*, International Meeting on LWR Fuel Performance, Orlando, Florida, USA, American Nuclear Society, 2004.

Andersson B. et al., *Advantages Gained by Introducing Low Tin ZIRLO™ as BWR Channel Material*, TopFuel 2015, Reactor Fuel Performance, Zurich, Switzerland, Eoropean Nuclear Society, pp 430-437, 2015.

Andriambololona H. et al., *Methodology for a Numerical Simulation of an Insertion or a Drop of the Rod Cluster Control Assembly in a PWR*, Nuclear Engineering and Design 237, 600–606, 2007.

ASME, *Boiler and Pressure Vessel Code, Section III - Rules for Construction of Nuclear Power Plant Components: Division 1.* New York, New York, USA, American Society of Mechanical Engineers, 2015.

Bacon D.J. et al., *Computer Simulation of Defect Production by Displacement Cascades in Metals*, Nuclear Instruments and Methods in Physics Research B, Vol. 102, pp. 37-46, 1995.

Barbéris P. et al., *CASTA DIVTM: Experiments and Modelling of Oxide Induced Deformation in Nuclear Components*, 15th ASTM International Symposium: Zirconium in the Nuclear Industry, Sunriver, OR, June 2007, SRP 1505, B. Kammenzind and M. Limbäck, eds., ASTM I, pp. 612-631, 2009.

Bathe K. J., *Finite Element Procedures in Engineering Analysis*, Prentice-Hall, Englewood Cliffs, New Jersey, 1982.

Bergmann U. and King J., *TRITON11™ - Westinghouse 11×11 BWR Fuel Design*, Top Fuel 2016, Boise, Idaho, USA, American Nuclear Society, 2016.

Bickel G.A. and Griffiths M., *Manufacturing Variability and Deformation for Zr-2.5Nb Pressure Tubes*, J. Nucl. Mater. Volume 383, Issues 1-2, No.15, pp. 9-13, 2008.

Billerey A. and Waeckel N., *Evolution Of Fuel Rod Support Under Irradiation Impact On The Mechanical Behaviour Of Fuel Assemblies*, Proc. Water Reactor Fuel Performance Meeting, Kyoto, Japan, October 2-6, 2005.

Blat-Yrieix M. et al., *Toward a Better Understanding of Dimensional Changes in Zircaloy-4: What is the Impact Induced by Hydrides and Oxide layer?*, 15th Zirconium in the Nuclear Industry, ASTM, Sunriver, OR, June 2007, SRP 1505, B. Kammenzind and M. Limbäck, eds., ASTM I, pp. 594-609, 2009.

Blavius D., Münch C-J. and Garner N., *Dimensional Behaviour of Fuel Channels – Update on the Operational Experiences and Evaluation Results*, KTG Jahrestagung Kerntechnik, Hamburg, 2008a

Blavius D et al., Dimensional Behaviour of Fuel Channels – *Update on the Operational Experience and Evaluation Results*, Proc. Annual Meeting on Nuclear Technology, Deutsches Atomforum, pp. 451-459, Hamburg, Germany, 2008b

Bossis P. et al., *In PWR Comprehensive Study of High Burn-up Corrosion and Growth Behaviour of M5 and Recrystallised Low-Tin Zircaloy-4*, 15th ASTM International Symposium: Zirconium in the Nuclear Industry, ASTM I, STP 1505, pp. 430-456, Sunriver, OR, June 25-27, 2009.

Buckley S. N., *Properties of Reactor Materials and the Effects of Irradiation Damage*, Butterworths, London, p. 443-449, 1961.

# List of Abbreviations

| | |
|---|---|
| appm | atomic parts per million |
| BWR | Boiling Water Reactor |
| CANDU | Canada Deuterium Uranium reactor |
| CHF | Critical Heat Flux |
| CWSR | Cold Worked, Stress Relieved |
| DNB | Departure from Nucleate Boiling |
| dpa | Displacements per atom |
| FEM | Finite Element Method |
| $f_i$ | Kearns texture factor in the principal material direction i, with i = longitudinal, normal and transverse to rolling, pilgering or drawing directions |
| PCMI | Pellet-Cladding Mechanical Interaction |
| PHWR | Pressurized Heavy Water Reactor |
| PWR | Pressurized Water Reactor |
| PRA | Partial Recrystallization Anneal |
| RXA | Recrystallization Anneal (generally applied to full recrystallization in the $\alpha$ phase region) |
| SPP | Second Phase Precipitate or Particle |
| SRA | Stress-Relief Anneal (same as CWSR) |
| TSSd | Terminal Solid Solubility for dissolution |
| TSSp | Terminal Solid Solubility for precipitation |
| wtppm | weight parts per million |

# Unit conversion

| TEMPERATURE | | |
|---|---|---|
| °C + 273.15 = K | °C × 1.8 + 32 = °F | |
| T(K) | T(°C) | T(°F) |
| 273 | **0** | 32 |
| 289 | 16 | 61 |
| 298 | 25 | 77 |
| 373 | **100** | 212 |
| 473 | **200** | 392 |
| 573 | **300** | 572 |
| 633 | 360 | 680 |
| 673 | **400** | 752 |
| 773 | **500** | 932 |
| 783 | 510 | 950 |
| 793 | 520 | 968 |
| 823 | 550 | 1022 |
| 833 | 560 | 1040 |
| 873 | **600** | 1112 |
| 878 | 605 | 1121 |
| 893 | 620 | 1148 |
| 923 | 650 | 1202 |
| 973 | **700** | 1292 |
| 1023 | 750 | 1382 |
| 1053 | 780 | 1436 |
| 1073 | **800** | 1472 |
| 1136 | 863 | 1585 |
| 1143 | 870 | 1598 |
| 1173 | **900** | 1652 |
| 1273 | **1000** | 1832 |
| 1343 | 1070 | 1958 |
| 1478 | 1204 | **2200** |

| Radioactivity | |
|---|---|
| **1 Sv** | = 100 Rem |
| **1 Ci** | = 3.7 × $10^{10}$ Bq = 37 GBq |
| **1 Bq** | = 1 $s^{-1}$ |

| MASS | |
|---|---|
| kg | lbs |
| 0.454 | **1** |
| **1** | 2.20 |

| DISTANCE | |
|---|---|
| x (µm) | x (mils) |
| 0.6 | 0.02 |
| 1 | 0.04 |
| 5 | 0.20 |
| **10** | 0.39 |
| 20 | 0.79 |
| 25 | 0.98 |
| 25.4 | **1.00** |
| **100** | 3.94 |

| PRESSURE | | |
|---|---|---|
| bar | MPa | psi |
| **1** | 0.1 | 14 |
| 10 | **1** | 142 |
| 70 | 7 | 995 |
| 70.4 | 7.04 | **1000** |
| **100** | 10 | 1421 |
| 130 | 13 | 1847 |
| 155 | 15.5 | 2203 |
| 704 | 70.4 | **10000** |
| **1000** | 100 | 14211 |

| STRESS INTENSITY FACTOR | |
|---|---|
| MPa√m | ksi√inch |
| 0.91 | **1** |
| **1** | 1.10 |